

Analysis of the trends in ambient methane in the Baltimore-Washington region and comparison to model output

Sayantana Sahu¹, Anna Karion², Israel Lopez-Coto², Xinrong Ren³, Ross J. Salawitch¹, and Russell R. R. Dickerson¹

¹University of Maryland, College Park

²National Institute of Standards and Technology

³University of Maryland and NOAA ARL

December 13, 2022

Abstract

We studied atmospheric methane observations from November 2016 to October 2017 from one rural and two urban towers in the Baltimore-Washington region (BWR). Methane observations at these three towers display distinct seasonal and diurnal cycles with maxima at night and in the early morning, reflecting local emissions and boundary layer dynamics. Peaks in winter concentrations and vertical gradients indicate strong local anthropogenic wintertime methane sources in urban regions. In contrast, our analysis shows larger local emissions in summer at the rural site, suggesting a dominant influence of wetland emissions. We compared observed enhancements (mole fractions above the 5th percentile) to simulated methane enhancements using the WRF-STILT model driven by two EDGAR inventories. When run with EDGAR 5.0, the low bias of modeled versus measured methane was greater (ratio of 1.9) than the bias found when using the EDGAR 4.2 emission inventory (ratio of 1.3). However, the correlation of modeled versus measured methane was stronger (~1.2 times higher) for EDGAR 5.0 compared to results found using EDGAR 4.2. In winter, the inclusion of wetland emissions using WETCHARTs had little impact on the mean bias, but during summer, the low bias for all hours using EDGAR 5.0 improved by from 63 to 23 nanomoles per mole of dry air or parts per billion (ppb) at the rural site. We conclude that both versions of EDGAR underestimate the regional anthropogenic emissions of methane, but version 5.0 has a more accurate spatial representation.

1 **Analysis of the trends in ambient methane in the Baltimore-Washington region and**
2 **comparison to model output**

3
4 *Sayantana Sahu¹, Anna Karion², Israel Lopez-Coto², Xinrong Ren³, Ross J. Salawitch^{1,4,5}, Russell R. Dickerson^{1,4,5}*

5
6 1. Department of Chemistry and Biochemistry, University of Maryland, College Park, Maryland, USA

7 2. National Institute of Standards and Technology, Gaithersburg, Maryland, USA

8 3. Air Resources Laboratory, National Oceanic and Atmospheric Administration, College Park, Maryland, USA

9 4. Department of Atmospheric and Oceanic Science, University of Maryland, College Park, Maryland, USA

10 5. Earth System Science Interdisciplinary Center, University of Maryland, College Park, Maryland, USA

11
12 Corresponding author: Sayantan Sahu ([sayantan@umd.edu](mailto:sayantana@umd.edu))

13
14 **Key Points:**

- 15
- 16 • Both versions of EDGAR (4.2 and 5.0) underestimate the regional anthropogenic emission of methane.
 - 17 • The correlation of modeled versus measured methane was stronger with the EDGAR
 - 18 5.0.
 - 19 • Inclusion of fluxes of wetland emissions reduce the bias between modeled and
 - 20 measured methane, especially in summer at the rural site.
- 21
22

23 **Abstract**

24 We studied atmospheric methane observations from November 2016 to October 2017 from one rural and two urban
25 towers in the Baltimore-Washington region (BWR). Methane observations at these three towers display distinct
26 seasonal and diurnal cycles with maxima at night and in the early morning, reflecting local emissions and boundary
27 layer dynamics. Peaks in winter concentrations and vertical gradients indicate strong local anthropogenic wintertime
28 methane sources in urban regions. In contrast, our analysis shows larger local emissions in summer at the rural site,
29 suggesting a dominant influence of wetland emissions. We compared observed enhancements (mole fractions above
30 the 5th percentile) to simulated methane enhancements using the WRF-STILT model driven by two EDGAR
31 inventories. When run with EDGAR 5.0, the low bias of modeled versus measured methane was greater (ratio of
32 1.9) than the bias found when using the EDGAR 4.2 emission inventory (ratio of 1.3). However, the correlation of
33 modeled versus measured methane was stronger (~1.2 times higher) for EDGAR 5.0 compared to results found
34 using EDGAR 4.2. In winter, the inclusion of wetland emissions using WETCHARTs had little impact on the mean
35 bias, but during summer, the low bias for all hours using EDGAR 5.0 improved by from 63 to 23 nanomoles per
36 mole of dry air or parts per billion (ppb) at the rural site. We conclude that both versions of EDGAR underestimate
37 the regional anthropogenic emissions of methane, but version 5.0 has a more accurate spatial representation.

38 **Plain Language Summary**

39
40 In this study we analyzed methane observations from three towers in the Baltimore-Washington region and used
41 these observations to evaluate anthropogenic and biogenic methane emission inventories. We found that
42 anthropogenic methane sources dominate at the urban sites while wetland emissions dominate at the rural site.
43 Significant discrepancies were observed between observations and methane outputs from a transport and dispersion
44 model run with different inventories, indicating substantially underestimated methane emissions in these inventories.
45 The low bias was greater with a newer version (EDGAR 5.0) than with an older version (EDGAR 4.2), however the
46 correlation was stronger with the newer version. We attribute the stronger correlation to improved spatial
47 distribution of methane emissions within the newer version. Adding wetland emissions reduced bias and improved
48 the seasonal cycle in modeled methane at the rural site.

49 **1. Introduction**

50 Methane is an important and not yet fully understood greenhouse gas, with a global warming potential of about 80
51 times more than carbon dioxide over a 20 year time horizon (Sixth Assessment Report — IPCC), although with an
52 atmospheric lifetime much shorter than carbon dioxide. There are both natural and anthropogenic sources of
53 methane. For example, natural sources include wetlands and wild animals while anthropogenic sources include the
54 production, transmission, distribution, and use of natural gas, as well as coal, livestock, wastewater treatment, and
55 landfills. In the United States (U.S.), natural gas and petroleum systems are the second largest source of methane
56 emissions after agriculture (Inventory of U.S. Greenhouse Gas Emissions and Sinks | U.S. EPA). Urban areas are a
57 significant source of anthropogenic methane emissions, often dominated by fugitive emissions from the natural gas
58 distribution and usage (Ren et al., 2018; Plant et al., 2019; Sargent et al., 2021).

59 Methane emissions from urban areas remain uncertain. Studies have attempted to assess and quantify the methane
60 emissions from natural gas leakage in urban centers and the transmission and storage (T&S) sector as a whole
61 (Alvarez et al., 2012, 2018; Peischl et al., 2013; Phillips et al., 2013; Jackson et al., 2014; Gallagher et al., 2015;
62 Kathryn et al., 2015; Lamb et al., 2015; Zimmerle et al., 2015; Hendrick et al., 2016; Cambaliza et al., 2017).
63 Substantial disparities exist between bottom-up estimates (inventories) and top-down estimates (based on
64 atmospheric measurements) with top-down estimates generally much larger than bottom-up values (Lamb et al.,
65 2016; Turner et al., 2016; Ren et al., 2018; Lopez-Coto et al., 2020). A recent study by Plant et al., (2019) used
66 aircraft measurements to conclude that methane emissions from many urban centers along the U.S. East Coast are
67 more than twice those in inventories. Ren et al., (2018) and Lopez-Coto et al., (2020) used airborne measurements to
68 determine that the winter (February) methane emission rates in 2016 in the Baltimore-Washington region (BWR)
69 were 2.7 to 2.8 times the US national greenhouse gas inventory for 2012. Huang et al., (2019), used atmospheric
70 inversions with methane observations from towers in the BWR and found methane emissions underestimated by the
71 existing inventories in fall, winter, and spring but overestimated in summer because of excess modeled wetland
72 emissions.

73 Few studies have looked at how models reproduce observed diurnal and seasonal trends of methane. Yadav et al.,
74 (2019) and He et al., (2019) used continuous observations (tower-based and remote-sensing, respectively) in the
75 Southern California air basin to show seasonality in urban methane emissions. Sargent et al., (2021) showed distinct
76 seasonality in methane emissions in Boston using in-situ observations in that city as well. Huang et al., (2019) used
77 data from afternoon hours (12 pm to 5 pm) and discovered a significant seasonality in urban methane emissions in
78 the BWR. The objective of our study is to evaluate anthropogenic and biogenic methane emission inventories with
79 ambient observations from towers. The aim is to better understand the sources and to evaluate existing inventories of
80 methane. We studied in-situ methane data from the BWR under the Northeast Corridor (NEC) project using two
81 urban towers ARL (Arlington, VA), NEB (Northeast Baltimore, MD), and one rural tower, BUC (Bucktown, MD)
82 (Karion et al., 2020). Karion et al., (2020) discussed methane measurements from two of these three towers – ARL
83 and BUC. The methane observations from these towers displayed distinct seasonal and diurnal cycles with seasonal
84 maxima in winter at the urban towers reflecting greater emissions and reduced vertical mixing, and larger vertical
85 gradients at night and early morning, indicating significant local emissions and higher concentrations when the
86 planetary boundary layer (PBL) is shallow. At BUC, the rural site, Karion et al., (2020) observed large vertical
87 gradients during the early morning hours in the summer, suggesting substantial local wetland emissions expected to
88 peak when the surface is warm. In our study, we compared modeled methane enhancements to observed
89 enhancements. We used the meteorological WRF (Weather Research and Forecasting) Model (Skamarock et al.,
90 2008) in combination with Lagrangian dispersion model STILT (Stochastic Time-Inverted Lagrangian Transport
91 model) (Lin et al., 2003; Nehrkorn et al., 2010) to simulate time series of methane at each tower location. We

92 compared the tower methane observations with the model outputs and used the ambient observations to evaluate the
93 anthropogenic and biogenic methane emission inventories.

94 **2. Methods**

95 **2.1. Tower locations and observations**

96 The NEC tower network, currently consisting of 29 stations, was initiated in 2015, with the primary objective to
97 better quantify urban emissions of anthropogenic greenhouse gases (Karion et al., 2020). Sixteen stations were
98 established around the BWR to estimate greenhouse gas emissions using inverse modeling techniques (Lopez-Coto
99 et al., 2017; Mueller et al., 2018). The tower network design and location under NEC, data collection, processing,
100 instrumentation, and calibration have been discussed in detail in earlier publications (Welp et al., 2013; Verhulst et
101 al., 2017; Lopez-Coto et al., 2017; Mueller et al., 2018; Karion et al., 2020). We used continuous, hourly
102 measurements of methane from the three towers in the region - NEB, ARL, and BUC. NEB is located in the city of
103 Baltimore, where the median household income is \$52,164, while ARL is in Arlington, VA, a moderately developed
104 suburb of Washington DC with over twice the median income of Baltimore (\$122,604) (U.S. Census Bureau). Both
105 are classified as urban towers (Karion et al., 2020). BUC is located in Bucktown, MD, on the eastern side of
106 Chesapeake Bay, in a wetland-dominant region (Karion et al., 2020). The location of these towers and the sampling
107 heights are provided in Table S1 & Figure S1, and also in Huang et al., (2019) and Karion et al., (2020).

108 We analyzed the diurnal and seasonal variation of methane at these three towers using contour plots as
109 previously done in Bloomer et al. (2010). We computed the hourly averages of the methane observations for each
110 month to generate these plots. We used data for the period November 2016 to October 2017 and focused our model
111 comparison analysis in two ecological seasons - winter (December 2016 to February 2017) and summer (June to
112 August 2017). Our research considered data from the entire diurnal cycle to determine how effectively the model
113 run with various inventories can replicate the observed diurnal trends. We used results from only the lower sampling
114 height (46m to 50 m above ground level) for the model bias comparison but obtained similar results when
115 considering data from the upper sampling height. Data from both sampling heights of each tower were used for the
116 vertical gradient analysis.

117

118 **2.2. Description of model and inventories**

119 Our study used the STILT transport and dispersion model (Lin et al., 2003b) run with meteorological data from
120 WRF model (Skamarock and Klemp, 2008; Skamarock et al., 2008) and configured as described in (Karion et al.,
121 2021). STILT was run 120 h backward in time from the observation points – the locations of the towers in our study.
122 The surface influence (proportional to the residence time of a particle over a given pixel and within the planetary
123 boundary layer) for each observation, or footprint, was calculated. The surface influence at each pixel was
124 multiplied by the emissions inventory's surface flux ($\mu\text{mol}/\text{m}^2/\text{s}$). The sum over all pixels equals the modeled mole
125 fraction enhancement at the tower site. Footprints were generated for each tower for a regional domain (bounds 92.0
126 W, 68.0 W, 33.0 N, 47.0 N) at 0.1-degree resolution. The domain is shown in Figure S2.

127 We used two anthropogenic CH₄ emission inventories – the Emission Database for Global Atmospheric Research
128 versions 4.2 (hereafter referred to as EDGAR 4.2) (Janssens-Maenhout et al., 2013) and 5.0 (hereafter referred to as
129 EDGAR 5.0) (EDGAR - Joint Research Centre Data Catalogue - EDGAR v5.0 Greenhouse Gas Emissions -
130 European Commission; Crippa et al., 2019) for 2012. The inventories have a horizontal resolution of 0.1° latitude by
131 0.1° longitude. There is no seasonality in methane emissions in EDGAR 4.2 and essentially no variation (< 5%) with
132 season in EDGAR 5.0 in our model domain or near our towers. Here, we used the annual average of emissions for a
133 particular year in the model. We chose these two versions of EDGAR because they have the most different spatial
134 representation of emissions, with EDGAR 4.2 placing more emissions in urban centers (i.e., emissions are
135 downscaled via population) than EDGAR 5.0. (Janssens-Maenhout et al., 2013). The distribution of methane
136 emissions within the inventories for the area near the towers is discussed in the results section.

137

138 **2.3. Comparison of observations and model outputs**

139 Our study considered several methods to compare modeled wetland emissions with observations. To
140 account for wetland methane emissions, we used wetland fluxes derived from WetCHARTs, with a horizontal
141 resolution of 0.5° latitude by 0.5° longitude (Bloom et al., 2017). WetCHARTs consists of 18 emission models, of
142 which nine exhibit higher magnitude of methane wetland fluxes than others, while the remaining 9 models are
143 significantly lower in magnitude and have different spatial allocations of wetland emissions (Figures S3a-b). We
144 calculated the mean from the 9 models with higher magnitude (hereafter referred to as ‘wet 3a’) and lower
145 magnitude (hereafter referred to as ‘wet 4a’) of wetland fluxes averaged monthly over 15 years. We also determined
146 the mean of all 18 models over 15 years (hereafter referred to as ‘wet ma’) for comparison with observations. In
147 addition to the three scenarios mentioned above (wet 3a, wet 4a and wet ma), we have downscaled the emissions to
148 our 0.1° model resolution using the wetland fraction (calculated as the sum of woody and herbaceous wetlands) from
149 the National Land Cover Database (NLCD) 2016 (Yang et al., 2018), conserving the mass within each 0.5° cell. We
150 have referred to the scenarios as ‘wet 3b’, ‘wet4b’, and ‘wet mb’.

151 We adopted a simple approach to directly compare the model outputs with methane tower observations.
152 The WRF-STILT model footprints are convolved (multiplied pixel by pixel and then summed) with inventories
153 (both anthropogenic and WetCHARTs) to simulate methane mole fraction enhancement in nanomoles of methane
154 per mole of dry air, (nmol mol⁻¹), or parts per billion (ppb), interpreted as excess methane over the atmospheric
155 background concentration. Due to the small number of towers used in this work and the fact that none of them could
156 really be considered a background tower, we decided to apply a simplified background methodology, treating each
157 tower independently, as opposed to more complex background methods as described in Karion et al., (2021). We
158 subtracted the 5th percentile, similarly to Pak et al., (2021) but determined seasonally for each tower, from the
159 absolute methane mole fractions from both the tower observations and the modeled output. We repeated our analysis
160 with the 2nd, 10th, and 15th percentile (Tables S2-3) subtracted from the methane tower observations and the model
161 results and found that while the choice of percentile impacts the magnitude of the biases it did not impact the
162 direction of the biases, the normalized mean bias (see below), nor the general conclusions; here, we presented results
163 using the 5th percentile.

164 We added the WetCHARTs modeled outputs to the EDGAR outputs (and subsequently deducted the 5th
 165 percentile) to determine if the inclusion of wetland emissions could bring better agreement between the model and
 166 observations. We used the bias and normalized mean bias (hereafter referred to as NMB) of methane to quantify the
 167 discrepancies between the model and observations. The NMB gives a good idea of how significant the bias is
 168 relative to the signal (enhancement). The two quantities were calculated as follows,

$$169 \text{ Mean bias (ppb methane)} = \frac{\sum_{i=1}^n (\text{model}_i - \text{obs}_i)}{n}$$

170 (Eq. 1)

$$171 \text{ Normalized mean bias (NMB)} = \frac{\sum_{i=1}^n (\text{model}_i - \text{obs}_i)}{\sum_{i=1}^n \text{obs}_i}$$

172 (Eq. 2)

173

174 (n = number of observations)

175

176 Here, ‘obs’ and ‘model’ refer to the observations and modeled output above the 5th percentile. A negative mean bias
 177 will be reflective of the model underestimating observations. We also calculated the least squares coefficient of
 178 determination (r^2) between methane observations and the model.

179 We investigated the methane vertical gradients between the two inlet heights at the three towers and
 180 compared these with model output. The analysis of vertical gradients will help understand whether the towers are
 181 located in the vicinity of sources (Monteiro et al., 2022). When the PBL is not well-mixed (e.g., at night or early
 182 morning), ground-level emissions near the tower result in higher concentrations at the lower level, thus larger
 183 gradients indicate higher emissions near the tower.

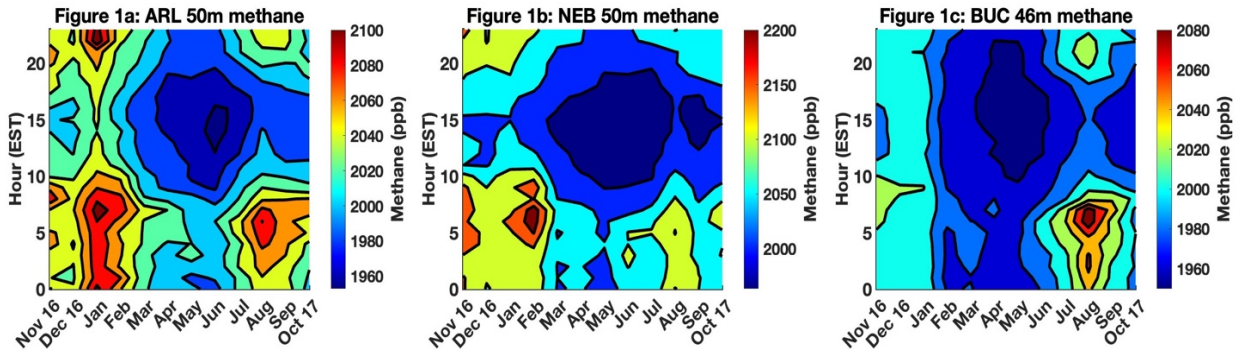
184 **3. Results**

185 **3.1. Analysis of methane observations at the three towers**

186 Methane measurements from the three towers in our study display distinct diurnal and seasonal cycles with daily
 187 maxima in the early morning and night hours (Figure 1). The presence of such distinct early morning and nighttime
 188 local maxima indicates local emissions. These maxima can be explained by the buildup from local emissions in the
 189 shallower boundary layer that are later dissipated due to turbulent mixing in the afternoon hours. The methane
 190 contour plots at the urban sites, NEB and ARL, show that this early morning enhancement is greatest during winter,
 191 but a secondary maximum in the early morning also appears in the late summer months (around August). The higher
 192 ambient concentration in the early morning and night hours in winter can be attributed to both enhanced
 193 anthropogenic methane emissions in winter and to the seasonality of boundary layer heights (Huang et al., 2019;
 194 Karion et al., 2020). Minima are observed in the summer afternoons when the PBL is deepest. The pattern indicates
 195 the importance of local emissions in the vicinity of the tower. The urban sites show a dominant winter peak
 196 suggesting that leakage from the natural gas (NG) system may be a major local source, if NG system emissions are

199 higher in winter than summer, as suggested by previous urban studies (He et al., 2019; Sargent et al., 2021). The
 200 secondary summer peak indicates that other, likely biogenic, sources may also be at play. Seasonality in
 201 meteorological conditions, including the PBL, also plays a role.

202



203

204

205 **Figure 1.** Methane contour plots showing diurnal and seasonal variation of methane at the three towers for the
 206 period November 2016 – October 2017. The data are from the lower inlet height of the towers 50 m above ground
 207 level for NEB and ARL and 46 m for BUC. Note the color bars are different in each plot.

208

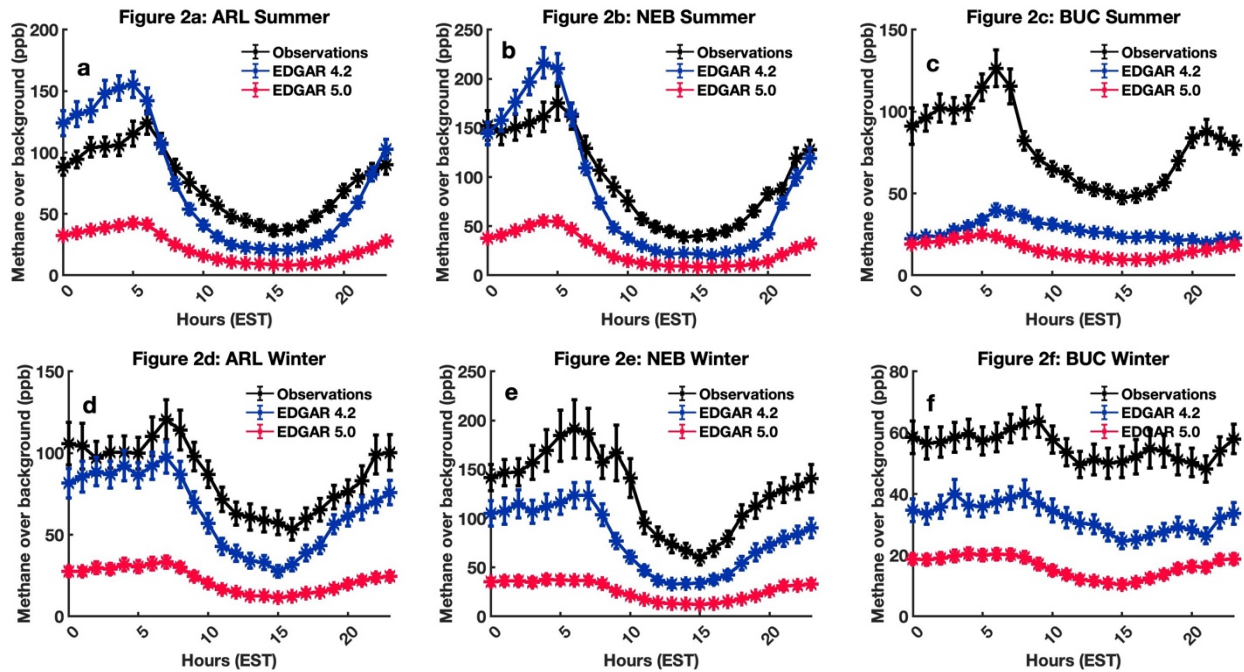
209 Unlike the urban sites, the rural BUC site shows a dominant early morning enhancement during the summer months,
 210 indicating a strong local biogenic process more pronounced at higher temperatures. This late summer maximum is
 211 coincident with the summer maxima discussed for the urban towers (ARL and NEB), indicating that these towers
 212 might also be impacted by biogenic sources. BUC is located in Dorchester County, MD, with close to 68,400
 213 hectares of estuarine and palustrine wetlands, besides agricultural land. This site shows a minor winter maximum
 214 likely related to PBL dynamics coupled with some minor emissions in winter. The absolute values of the methane
 215 mole fractions are greatest at NEB and smallest at BUC. These patterns suggest that urban methane emissions are
 216 greater than rural emissions in the BWR.

217

218 3.2. Comparison of observed and modeled diurnal cycles of methane

219 We analyzed both the observed and modeled diurnal variations of methane enhancements at all three towers to
 220 investigate how accurately the models captured the observed diurnal trends of methane. The modeled outputs were
 221 derived from the WRF-STILT runs with the EDGAR inventories as described in the Methods section. The plots in
 222 Figures 2a-f show the observed diurnal cycles of methane enhancements plotted along with the WRF-STILT model
 223 predicted diurnal cycles, run with EDGAR 4.2 or EDGAR 5.0.

224



225

226

227

228 **Figure 2.** Diurnal cycles of methane enhancements during summer (a-c) and winter months (d-f) at two urban
 229 towers, ARL and NEB, and one rural tower, BUC. The black line represents the hourly averaged methane
 230 observations; the blue and red lines represent modeled diurnal trends run with EDGAR 4.2 and EDGAR 5.0
 231 inventories respectively using the 5th percentile as background. The error bars represent the standard error of the
 232 mean, i.e., the standard deviation of the hourly observations divided by the square root of the number of
 233 observations used to calculate the mean.

234

235 3.2.1. Analysis of observed diurnal cycles of methane

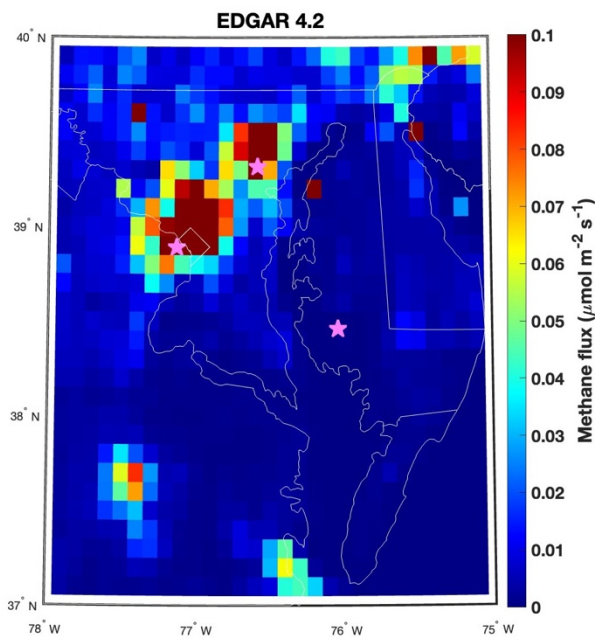
236 The observed diurnal cycles of methane enhancements for the three sites displayed a pronounced maximum in the
 237 early morning and the night, as also shown in Figure 1 and suggesting local emissions. As explained earlier, local
 238 emissions produce maxima in concentrations when the PBL is shallow. At the two urban sites, the magnitude of
 239 observed early morning maximum was greater during the winter than the summer. A plausible reason could be
 240 greater local anthropogenic methane emissions during winter due to increased NG use for heating, resulting in a
 241 higher early morning maximum in the diurnal cycle (He et al., 2019; Sargent et al., 2021), but also possibly caused
 242 by lower mixing layer depths in winter compared to summer. At BUC, a prominent diurnal cycle was seen during
 243 summer with a weaker variation during winter, suggesting that it is influenced by strong summer-time local sources,
 244 while winter-time enhancements originated farther from the tower, or by weak, local sources. Figure 1b shows
 245 evidence of strong seasonal emissions, likely from wetlands, at BUC that may explain the diurnal cycle in summer
 246 and near absence of it in winter.

247

248 3.2.2. Analysis of modeled diurnal cycles of methane to determine model - observation bias

249 It is evident from Figures 2a-f that significant discrepancies exist between the modeled and observed enhancements
 250 at all three towers. The WRF-STILT runs with both EDGAR inventories underestimate the enhancement of methane
 251 substantially in most cases at all three sites. EDGAR does not include wetland emissions of methane, which can
 252 plausibly explain the discrepancies between model and methane observations, especially in summer. WRF-STILT
 253 driven with the EDGAR 5.0 inventory has a greater negative bias relative to methane observations than when driven
 254 with EDGAR 4.2. In general, the EDGAR 4.2 inventory appears to reproduce the observed diurnal trend better (with
 255 less bias) than EDGAR 5.0.

256 In the winter, both EDGAR inventories underestimate methane during all hours, at all three towers. This is
 257 clear evidence of the model underestimating anthropogenic methane emissions, as we do not expect large natural
 258 emissions from wetlands in winter. The bias is greater with EDGAR 5.0 than with EDGAR 4.2, however. The
 259 spatial distributions of methane emissions within the area near the towers for both EDGAR 4.2 and EDGAR 5.0 are
 260 shown in Figures 3a-b. The total methane emissions within this area are significantly higher in EDGAR 4.2 (a factor
 261 of 1.85 in the area shown in Figure 3) compared to EDGAR 5.0. In addition, EDGAR 4.2 has more concentrated
 262 emissions around the cities, which strongly influence observations at the urban sites. These factors combined result
 263 in higher modeled enhancements relative to EDGAR 5.0 and thus lower bias. Both EDGAR inventories
 264 underestimate observed methane enhancements at BUC during winter, when wetland emissions are minimal,
 265 suggesting that these inventories also underestimate anthropogenic methane emissions upwind of this rural site. The
 266 bias is lower, in absolute magnitude, during the afternoon hours, when the boundary layer is well mixed, than at
 267 other times of the day, but still substantial.
 268



269
270
271
Figure 3a

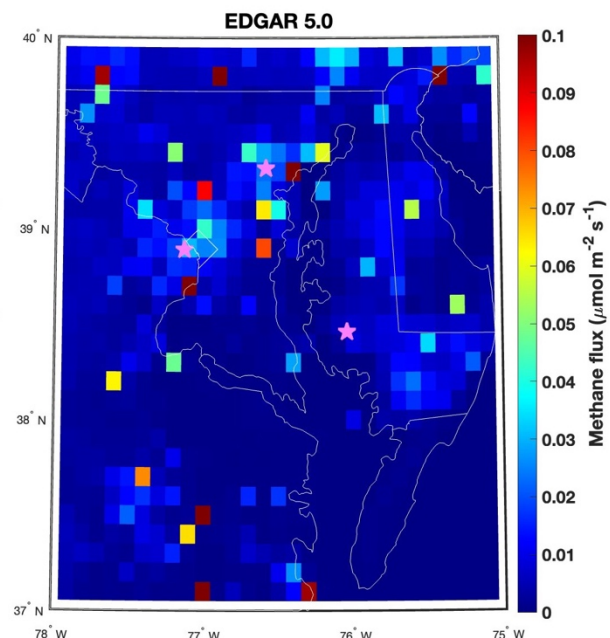


Figure 3b

272 **Figures 3.** Distribution of CH₄ emission fluxes (in units of $\mu\text{mol}/\text{m}^2/\text{s}$) in EDGAR 4.2 (left) and EDGAR 5.0 (right)
 273 around the towers used in our analysis. The pink stars represent the towers in our study. Color axis has been
 274 truncated for clarity.

275
 276 At the urban towers during the summer months, EDGAR 5.0 underestimates methane observed enhancements at all
 277 hours. However, EDGAR 4.2 underestimates methane enhancements during afternoon hours but overestimates them
 278 during early morning hours. A plausible explanation of the overestimation could be lower emissions of methane
 279 during summer compared to winter (Huang et al., 2019), combined with potential inaccurate representation of
 280 planetary boundary layer dynamics in the transport model. Emissions of methane within EDGAR versions used here
 281 are averaged annually, so there is no temporal variability in the anthropogenic emissions used in the model. During
 282 the summer months at BUC, the rural site in an area of extensive estuaries and other wetlands, significant
 283 discrepancies between the modeled and observed enhancements exist at all hours. This can be explained by the fact
 284 that EDGAR inventories do not include natural (wetland) emissions, discussed below.

285

286 3.2.3. Mean bias, NMB, correlation between observed and modeled methane enhancements

287 To quantify the bias between model outputs and observed methane enhancements, we analyzed the mean bias (Eq.
 288 1), normalized mean bias (NMB, Eq. 2), and the coefficient of determination (r^2). The results for summer and winter
 289 afternoon hours (12 pm to 3 pm EST) are tabulated in Table 1 and all hours in Table S4.

290

291

292 **Table 1**

293 *Mean bias (in ppb of methane, i.e., nmol/mol), normalized mean bias, and r^2 between modeled and observed*
 294 *enhancements for winter and summer afternoon hours, using the 5th percentile background.*

295

Tower	Inventory	Season	Mean bias (ppb)	NMB	r^2
BUC	EDGAR 4.2	winter	-22.26	-0.44	0.26
NEB		winter	-42.50	-0.52	0.38
ARL		winter	-26.97	-0.40	0.33
BUC	EDGAR 5.0	winter	-37.50	-0.74	0.29
NEB		winter	-65.93	-0.80	0.39
ARL		winter	-51.78	-0.77	0.36
BUC	EDGAR 4.2	summer	-35.10	-0.60	0.30
NEB		summer	-26.98	-0.49	0.18
ARL		summer	-18.78	-0.39	0.28
BUC		summer	-46.38	-0.80	0.36

NEB	EDGAR 5.0	summer	-43.39	-0.79	0.22
ARL		summer	-36.40	-0.75	0.36

296

297 *Note.* The corresponding table for all hours is in Table S4.

298

299 On average, the modeled methane enhancements are biased low in winter by approximately 22 ppb to 37 ppb at
300 BUC, and by 27 ppb to 66 ppb for the urban towers (NEB and ARL), depending on which EDGAR inventory is
301 used. The bias is greater for the urban towers compared with the rural site, and greater with EDGAR 5.0 than with
302 4.2 at all sites. During summer, the low bias ranges from approximately 19 ppb to 46 ppb when considering the three
303 towers. There is a greater low bias at the urban towers (NEB and ARL) during winter than at BUC. Conversely
304 during summer, the model low bias was greater at BUC than at the two urban towers. We attribute these tendencies
305 to weak wetland emissions during winter at the rural site that are amplified during summer. The urban towers are
306 influenced by the local anthropogenic methane emissions, likely from the NG distribution system or end usage,
307 which recent studies have suggested are higher in winter (He et al., 2019; Huang et al., 2019; Sargent et al., 2021).
308 Moreover, during winter, local emissions have a greater impact on observed enhancements due to the shallower
309 boundary layer. We arrive at the same conclusions when considering all hours of the day (Table S4). The low bias is
310 reduced to 1 ppb to 10 ppb of methane at the urban towers during summer when using EDGAR 4.2 due to the
311 overestimation by the model at early morning hours (Figures 2a-b). The bias is the smallest when only afternoon
312 hours are considered, possibly due to the smaller overall enhancements and because the transport model may
313 perform better under well-mixed conditions.

314 We compare the coefficient of determination (r^2) between modeled and observed CH₄ enhancements within
315 each season. Modeled methane from EDGAR 5.0 correlates better with observations than EDGAR 4.2 in most cases
316 despite the greater low bias, likely due to the improved spatial distribution of methane emissions in the newer
317 version. However, while EDGAR 5.0 correlates better with observations, it has a greater negative bias because it has
318 lower emissions, especially around urban centers. We note here that although a newer version of EDGAR (6.0) is
319 now available, it is very similar in both magnitude and spatial distribution to EDGAR 5.0 (Figure S4), so we would
320 not expect its use to yield any significant difference in our results.

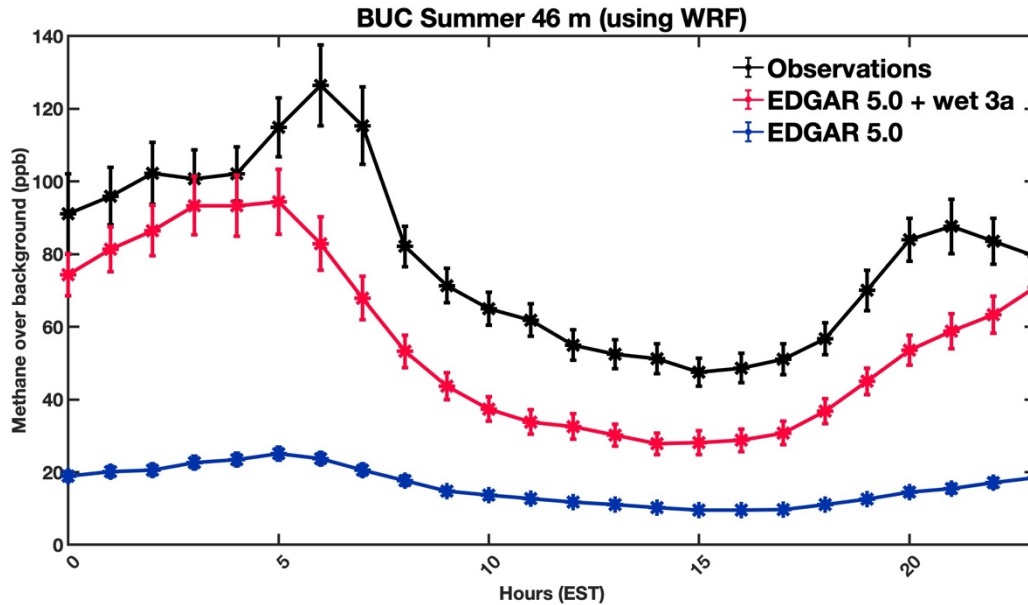
321

322 3.3. Incorporating wetland emissions using WETCHARTs

323 The summer concentration peak at BUC (an area of extensive estuaries and other wetlands) suggests strong natural
324 flux from wetlands, which are not included in the EDGAR anthropogenic emissions inventory. We thus ran the
325 model with WetCHARTs version 1.3.1 and added the resulting modeled enhancements from wetland emissions to
326 the anthropogenic enhancements from EDGAR 5.0 (See Figure 4, S5a-b and Tables S7-10). We used WRF-STILT
327 outputs with EDGAR 5.0 rather than 4.2 as EDGAR 5.0 better correlated with observations. Our findings suggest
328 that during winter, the addition of various WetCHARTs combinations has little impact on the bias, as expected
329 (wetland emissions are very small in winter (Figure S3)). The combinations ‘wet 3a’ and ‘wet 3b’ produce the
330 smallest bias under all scenarios, as these include the WetCHARTs members that have significantly higher methane

331 flux than others. During winter afternoon hours, the model was still biased low by approximately 35 ppb, 63 ppb, 50
 332 ppb at BUC, NEB, and ARL, respectively. The continued underestimation by the model during winter after
 333 incorporating wetland emissions is clear evidence of EDGAR 5.0 underestimating anthropogenic emissions of
 334 methane in this region.

335



336

337

338 **Figure 4:** Diurnal cycle of methane at BUC during summer. The black line represents the hourly averaged methane
 339 observations. The red and blue lines represent the model predicted diurnal trends using the EDGAR 5.0 inventory,
 340 with and without wetland emissions, respectively. The error bars represent the standard error of the mean of the data
 341 in hourly bins.

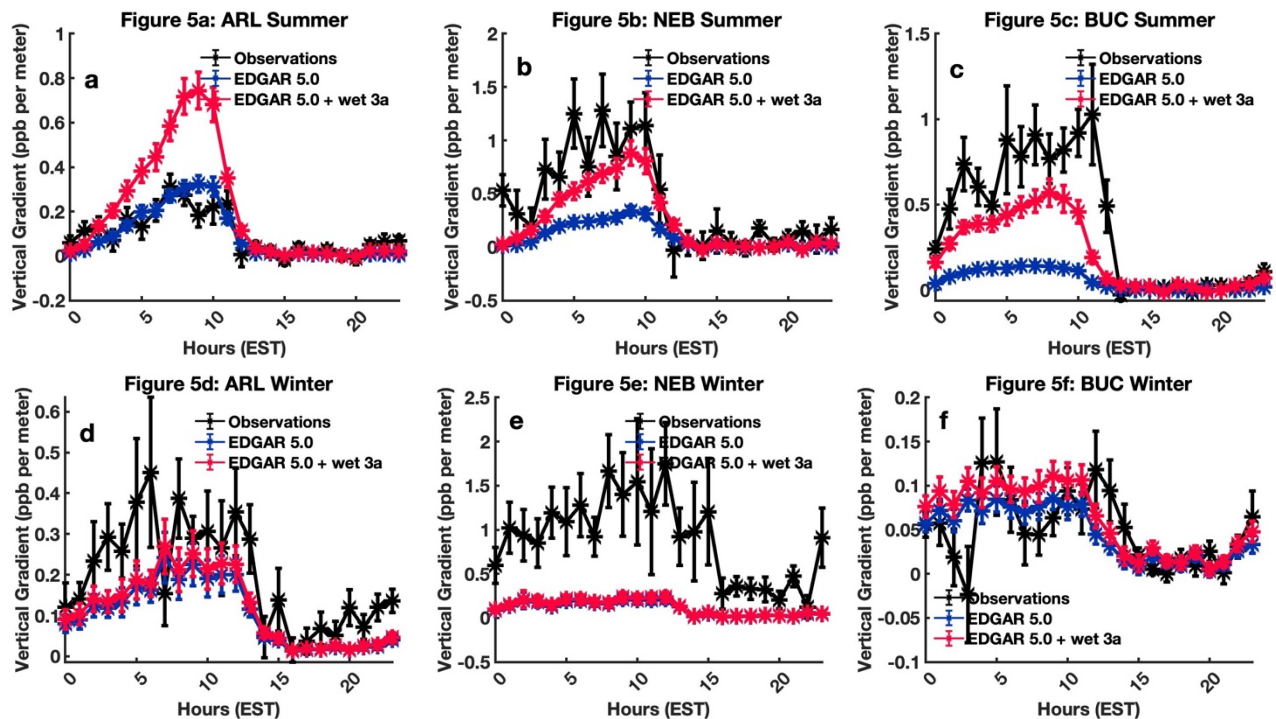
342

343 In summer, we observe much better agreement between modeled and observed CH₄ enhancements after including
 344 the effect of wetland emissions in the model. The negative model bias falls to approximately 20 ppb during
 345 afternoon hours at the three towers and ranges from approximately 12 to 28 ppb when considering all hours. Thus,
 346 even after adding wetland emissions in summer, a substantial bias remains, suggesting that WetCHARTs either
 347 underestimates the magnitude of wetland emissions or that the anthropogenic underestimation is so large that it is
 348 not compensated for by including wetland emissions. Adding WetCHARTs improves the seasonal cycle in modeled
 349 CH₄ at BUC as the summer afternoon low bias improves from approximately 46 ppb to 20 ppb. We compare the
 350 correlation (Tables S7-10) for the summer and winter seasons after adding modeled methane enhancements from
 351 WetCHARTs and find no improvement. The above observations show that WetCHARTs can be improved in both
 352 magnitude and spatial allocation of wetland emissions of methane.

353

354 **3.4. Analysis of observed and modeled Vertical gradient of methane**

355 We compared the observed and modeled vertical gradient of methane at the three towers for the winter and summer
 356 months. The vertical gradient was calculated as the difference in methane observations between the lower and the
 357 upper height, divided by the difference in inlet heights. A weak vertical gradient is indicative of a better mixed
 358 boundary layer or absence of strong local sources and sinks. When the boundary layer is not well-mixed, the
 359 gradient shows if there are local sources. The vertical gradient can help us better understand if strong local sources
 360 of methane influence the tower observations (Wyngaard et al., 1984; Dyer, 1974; Patton, Sullivan and Davis, 2003;
 361 Monteiro et al., 2022). However, the difference between modeled and observed vertical gradients is a function of
 362 both the accuracy of the emissions used in the model and the ability of the transport and dispersion model to
 363 simulate vertical mixing accurately. Figure 5 shows the diurnal variations of the observed and modeled vertical
 364 gradients at the three towers in summer (Figures 5a-c) and winter (Figures 5d-f).
 365



366
367
368

369 **Figure 5.** Vertical gradients of methane at the three towers in summer (a-c) and in winter (d-f). The black lines
 370 represent observed vertical gradient between the two inlet heights at the towers. The blue and the red lines represent
 371 the model simulated vertical gradient without wetland emissions and with ‘wet 3a’ emissions from WetCHARTs,
 372 respectively. The error bars represent the standard error of mean of vertical gradients in hourly bins.

373
374 **3.4.1. Observed Vertical gradient of methane**

375 We observe a large vertical gradient at both urban towers in the early morning hours that plummets in the afternoon
 376 hours (consistent with the early morning concentration maximum seen in Figure 1). The strong vertical gradient in
 377 the morning hours indicates that the towers are situated in the vicinity of methane sources. The pattern is similar
 378 during winter and summer; however, the morning vertical gradient is slightly higher during winter, which can be

379 attributed either to the seasonality of the nocturnal vertical mixing or greater anthropogenic methane emissions
380 during winter or both. In contrast, at BUC, we observe strong vertical gradients during summer, but they are close to
381 zero during winter indicating that local sources during this season are very weak. The strong summer vertical
382 gradients can be explained by local wetland emissions influencing observations at this site, and the bulk of
383 anthropogenic sources being farther away.

384

385 **3.4.2. Modeled Vertical gradient of methane**

386 We analyzed how reliably WRF-STILT run with EDGAR 5.0 can reproduce the observed vertical gradients at the
387 three towers. We included modeled methane enhancements from WetCHARTs “3a” (the mean of the high-emission
388 members) to account for biogenic emissions, because the “3a” version better matched summer observations at BUC
389 in our previous analysis. The discrepancy between observed and modeled vertical gradients at all three sites is
390 lowest during the late afternoon hours when the boundary layer is well-mixed. The results are congruent with the
391 results in the previous section, where we compared the observed and model-simulated diurnal patterns of methane
392 enhancements. At NEB and ARL, the inclusion of wetland emissions during winter does not substantially improve
393 the model bias, as they are very small in winter (see Tables S7-8). At ARL, during winter, we observed good
394 agreement between model outputs and observations, with a bias of approximately 0.1 ppb per meter during early
395 morning hours and less than 0.1 ppb per meter during the afternoon. At NEB, the model was biased low by
396 approximately 1 ppb per meter in the early morning hours and approximately 0.2 ppb per meter during the afternoon
397 hours, most likely due to local sources being underestimated in EDGAR 5.0.

398 During summer, at ARL, the model run with EDGAR 5.0 reproduces the observed diurnal trend in vertical
399 gradient remarkably well; however, the inclusion of wetland emissions overestimates the early morning gradient. In
400 contrast, at NEB during summer, the model simulations with the addition of wetland emissions significantly reduce
401 the bias between the modeled and observed vertical gradient, from approximately 1 to 0.2 ppb per meter. Thus,
402 either wetland emissions are influencing observations at NEB in summer, or (more likely, given the lack of nearby
403 wetlands) the additional modeled emissions are compensating for the large under-estimation of anthropogenic
404 emissions in EDGAR 5.0 at this site. At BUC, during winter, in the absence of any strong local sources, we observe
405 good agreement between model outputs and observations at all hours. During summer, when wetland emissions are
406 greatest, the addition of WetCHARTs output in the model significantly reduces the bias, especially during morning
407 hours, when local emissions are most significant.

408

409 **3.5. Contrasting urban sites - NEB and ARL**

410 When we compare the methane diurnal cycle at the two urban towers, we find greater methane enhancements at
411 NEB when compared to ARL. The absolute methane mole fractions are also greater at NEB than ARL (Figures 1a-
412 b). This may be the result of ARL being generally more upwind of the BWR and NEB being more generally
413 downwind, or to greater emissions near NEB, possibly due to fugitive methane emissions from leaks in the delivery
414 system (Weller, Hamburg and von Fischer, 2020). In this paper, we have pointed out the potential impact of natural
415 gas on observations, but local sources could also be from urban wastewater treatment and landfills.

416 Demographics and infrastructure may play a role in the differences of methane concentrations at the two
417 sites. The observation raises a pertinent question of environmental justice (Weller et al., 2022), as methane
418 concentrations may correlate with higher concentrations of other pollutants that affect health outcomes; future
419 studies should further investigate differences in methane sources and emissions magnitudes in these two cities
420 (Arlington, VA and Baltimore, MD). When comparing observations to modeled enhancements, we discover more
421 extreme bias toward low values in the model for the NEB than ARL (NMB 0.80 vs 0.77 for winter afternoon with
422 EDGAR 5.0), see Table 1. The difference can be because EDGAR 5.0 emissions are too low near NEB but more
423 accurate near ARL, compared to observed data, as also suggested by the vertical gradients.

424 **5. Conclusions**

425 Our study compared methane observations from three towers with output from a Lagrangian model using diurnal
426 patterns and vertical gradients. Results suggest that anthropogenic methane emissions dominate in the urban areas
427 (sites NEB and ARL) while natural (i.e., wetland) sources dominate at the rural site (BUC). Significant
428 discrepancies were found between models driven by EDGAR and observations; while EDGAR 5.0 seems to have an
429 improved spatial distribution of emissions (as suggested by higher correlations with observed enhancements), its
430 emissions magnitude in these two cities is too low. EDGAR 4.2, with larger urban emissions, compared more
431 favorably with observations in terms of magnitude. Both daily cycle and vertical gradient comparisons point toward
432 higher local emissions near NEB relative to ARL and higher emissions during winter than in summer at these urban
433 sites, although more work is needed to confidently conclude this. In addition, adding wetland emissions from
434 WetCHARTs significantly improved the agreement between modeled and observed vertical gradients especially in
435 summer at BUC. While adding wetland emissions from WetCHARTs reduced discrepancies in terms of bias,
436 especially in summer, the lower correlation observed might indicate that the distribution of these emissions could
437 still be improved and that we need better wetland models with greater resolution to replicate observations from the
438 mid-Atlantic wetland region. Besides the known anthropogenic emissions, we found evidence of additional summer
439 (possibly biogenic) emissions at the urban sites based upon analyses of the seasonal and temporal patterns of
440 observed methane. Future studies should investigate the source of summertime emissions around these sites and the
441 strength of these sources relative to the anthropogenic source of methane. We note that here we have investigated
442 CH₄ observations near towers using a simple seasonal background; a more quantitative determination of CH₄
443 emissions would require a more sophisticated treatment of background (e.g., Karion et al., 2021) and likely a higher
444 resolution modeling framework. Finally, future measurements of ethane and ¹³C isotopic analysis along with
445 methane might help distinguish the relative strength of biogenic and anthropogenic sources.

446 **Acknowledgments and Data Availability**

447 The authors thank Anthony Bloom (JPL) for providing the WetCHARTs v1.3.1 emissions product and NIST for
448 funding this project (Project code: 70NANB18H16; Award Number: 70NANB22H219). We thank Kimberly
449 Mueller (NIST) for providing us with model convolutions. Northeast Corridor tower methane observations are
450 available at <https://doi.org/10.18434/M32126> (Karion et al., 2019).

451

452 **Open Research**

453 Methane observations from the Northeast Corridor tower network can be found at
 454 <https://doi.org/10.18434/M32126> (Karion et al., 2019). STILT model data have been described in Lin et al
 455 2003b (<https://doi.org/10.1029/2002JD003161>), and the WRF model data have been described in Skamarock et
 456 al 2008 (<http://dx.doi.org/10.5065/D68S4MVH>). The EDGAR 4.2 data have been obtained from
 457 <http://data.europa.eu/89h/jrc-edgar-emissiontimeseriesv42> and the EDGAR 5.0 have been obtained from
 458 <http://data.europa.eu/89h/488dc3de-f072-4810-ab83-47185158ce2a>. WetCHARTs is described in Bloom et al.,
 459 (2017).

460

461 **References**

- 462 Alvarez, R.A. *et al.* (2012). Greater focus needed on methane leakage from natural gas infrastructure, *Proceedings*
 463 *of the National Academy of Sciences of the United States of America*, 109(17), pp. 6435–6440.
 464 <https://doi.org/10.1073/PNAS.1202407109>
- 465 Alvarez, R.A. *et al.* (2018). Assessment of methane emissions from the U.S. oil and gas supply chain. *Science*,
 466 361(6398), pp. 186–188. <https://doi-org.proxy-um.researchport.umd.edu/10.1126/science.aar7204>
- 467 Bloom, A. *et al.* (2017). A global wetland methane emissions and uncertainty dataset for atmospheric chemical
 468 transport models (WetCHARTs version 1.0). *Geoscientific Model Development*, 10(6), pp. 2141–2156.
 469 <https://doi.org/10.5194/GMD-10-2141-2017>
- 470 Bloomer, B.J., Vinnikov, K.Y. and Dickerson, R.R. (2010). Changes in seasonal and diurnal cycles of ozone and
 471 temperature in the eastern U.S. *Atmospheric Environment*, 44(21–22), pp. 2543–2551.
 472 <https://doi.org/10.1016/J.ATMOSENV.2010.04.031>
- 473 Cambaliza, M.O.L. *et al.* (2015). Quantification and source apportionment of the methane emission flux from the
 474 city of Indianapolis. *Elementa*, 3. <https://doi.org/10.12952/JOURNAL.ELEMENTA.000037>
- 475 Crippa, M. *et al.* (2019). EDGAR v5.0 Greenhouse Gas Emissions. European Commission, Joint Research Centre
 476 (JRC) [Dataset] PID: <http://data.europa.eu/89h/488dc3de-f072-4810-ab83-47185158ce2a>
- 477 Dyer, A.J. (1974). A review of flux-profile relationships,” *Boundary-Layer Meteorology* 1974 7:3, 7(3), pp. 363–
 478 372. <https://doi.org/10.1007/BF00240838>
- 479 *EDGAR - The Emissions Database for Global Atmospheric Research*.
 480 https://edgar.jrc.ec.europa.eu/index.php/dataset_ghg50 (Accessed: May 15, 2022).
- 481 Gallagher, M.E. *et al.* (2015). Natural Gas Pipeline Replacement Programs Reduce Methane Leaks and Improve
 482 Consumer Safety. *Environmental Science & Technology Letters*, 2(10), pp. 286–291.
 483 <https://doi.org/10.1021/acs.estlett.5b00213>
- 484 He, L. *et al.* (2019). Atmospheric Methane Emissions Correlate with Natural Gas Consumption from Residential and
 485 Commercial Sectors in Los Angeles. *Geophysical Research Letters*, 46(14), pp. 8563–8571.
 486 <https://doi.org/10.1029/2019GL083400>
- 487 Hendrick, M.F. *et al.* (2016). Fugitive methane emissions from leak-prone natural gas distribution infrastructure in
 488 urban environments. *Environmental Pollution*, 213, pp. 710–716.
 489 <https://doi.org/10.1016/J.ENVPOL.2016.01.094>
- 490 Horst, T.W. (1999). The footprint for estimation of atmosphere-surface exchange fluxes by profile techniques.
 491 *Boundary-Layer Meteorology*, 90(2), pp. 171–188. <https://doi.org/10.1023/A:1001774726067>
- 492 Huang, Y. *et al.* (2019). Seasonally Resolved Excess Urban Methane Emissions from the Baltimore/Washington,
 493 DC Metropolitan Region. *Environmental Science and Technology*, 53(19), pp. 11285–11293.
 494 <https://doi.org/10.1021/acs.est.9b02782>

- 495 *Inventory of U.S. Greenhouse Gas Emissions and Sinks* | US EPA. [https://www.epa.gov/ghgemissions/inventory-us-](https://www.epa.gov/ghgemissions/inventory-us-greenhouse-gas-emissions-and-sinks)
 496 [greenhouse-gas-emissions-and-sinks](https://www.epa.gov/ghgemissions/inventory-us-greenhouse-gas-emissions-and-sinks) (Accessed: March 28, 2022).
- 497 Jackson, R.B. *et al.* (2014). Natural gas pipeline leaks across Washington, DC. *Environmental Science and*
 498 *Technology*, 48(3), pp. 2051–2058.
 499 https://doi.org/10.1021/ES404474X/ASSET/IMAGES/ES404474X.SOCIAL.JPEG_V03
- 500 Janssens-Maenhout, G. *et al.* (2011). Emissions Database for Global Atmospheric Research, version v4.2 (time-
 501 series). European Commission, Joint Research Centre (JRC) [Dataset] PID: [http://data.europa.eu/89h/jrc-](http://data.europa.eu/89h/jrc-edgar-emissiontimeseriesv42)
 502 [edgar-emissiontimeseriesv42](http://data.europa.eu/89h/jrc-edgar-emissiontimeseriesv42)
- 503 Janssens-Maenhout, G. *et al.* (2013). Global emission inventories in the Emission Database for Global Atmospheric
 504 Research (EDGAR)—Manual (I). *publications.jrc.ec.europa.eu*.
 505 <https://doi.org/10.2788/81454>
- 506 *Joint Research Centre Data Catalogue - EDGAR v5.0 Greenhouse Gas Emissions - European Commission*.
 507 <https://data.jrc.ec.europa.eu/dataset/488dc3de-f072-4810-ab83-47185158ce2a> (Accessed: May 15, 2022).
- 508 Karion, A. *et al.* (2019). Observations of CO₂, CH₄, and CO mole fractions from the NIST Northeast Corridor
 509 urban testbed. <https://doi.org/10.18434/M32126>
- 510 Karion, A. *et al.* (2020). Greenhouse gas observations from the Northeast Corridor tower network. *Earth System*
 511 *Science Data*, 12(1), pp. 699–717. <https://doi.org/10.5194/ESSD-12-699-2020>
- 512 Lamb, B.K. *et al.* (2015). Direct measurements show decreasing methane emissions from natural gas local
 513 distribution systems in the United States. *Environmental Science and Technology*, 49(8), pp. 5161–5169.
 514 <https://doi.org/10.1021/es505116p>
- 515 Lamb, B.K. *et al.* (2016). Direct and Indirect Measurements and Modeling of Methane Emissions in Indianapolis,
 516 Indiana. *Environmental Science and Technology*, 50(16), pp. 8910–8917.
 517 <https://doi.org/10.1021/acs.est.6b01198>
- 518 Lin, J.C. *et al.* (2003a). A near-field tool for simulating the upstream influence of atmospheric observations: The
 519 Stochastic Time-Inverted Lagrangian Transport (STILT) model. *Journal of Geophysical Research:*
 520 *Atmospheres*, 108(D16), p. 4493. <https://doi.org/10.1029/2002JD003161>
- 521 Lin, J.C. *et al.* (2003b). A near-field tool for simulating the upstream influence of atmospheric observations: The
 522 Stochastic Time-Inverted Lagrangian Transport (STILT) model. *Journal of Geophysical Research:*
 523 *Atmospheres*, 108(D16), p. 4493. <https://doi.org/10.1029/2002JD003161>
- 524 Lopez-Coto, I. *et al.* (2017). Tower-based greenhouse gas measurement network design—The National Institute of
 525 Standards and Technology Northeast Corridor Testbed. *Advances in Atmospheric Sciences 2017 34:9*,
 526 34(9), pp. 1095–1105. <https://doi.org/10.1007/S00376-017-6094-6>
- 527 Lopez-Coto, I. *et al.* (2020). Wintertime CO₂, CH₄, and CO Emissions Estimation for the Washington, DC–
 528 Baltimore Metropolitan Area Using an Inverse Modeling Technique. *Environmental Science &*
 529 *Technology*, 54(5), 2606–2614. <https://doi.org/10.1021/acs.est.9b06619>
- 530 McKain, K. *et al.* (2015). Methane emissions from natural gas infrastructure and use in the urban region of Boston,
 531 Massachusetts. *Proceedings of the National Academy of Sciences of the United States of America*, 112(7),
 532 pp. 1941–1946. <https://doi.org/10.1073/PNAS.1416261112>
- 533 Monteiro, V. *et al.* (2022). The impact of the COVID-19 lockdown on greenhouse gases: a multi-city analysis of in
 534 situ atmospheric observations. *Environmental Research Communications*, 4(4), p. 041004.
 535 <https://doi.org/10.1088/2515-7620/AC66CB>
- 536 Mueller, K. *et al.* (2018). Siting Background Towers to Characterize Incoming Air for Urban Greenhouse Gas
 537 Estimation: A Case Study in the Washington, DC/Baltimore Area. *Journal of Geophysical Research:*
 538 *Atmospheres*, 123(5), pp. 2910–2926. <https://doi.org/10.1002/2017JD027364>
- 539 Nehr Korn, T. *et al.* (2010). Coupled weather research and forecasting—stochastic time-inverted Lagrangian transport
 540 (WRF–STILT) model. *Meteorology and Atmospheric Physics 2010 107:1*, 107(1), pp. 51–64.
 541 <https://doi.org/10.1007/S00703-010-0068-X>
- 542 Pak, N. *et al.* (2021). The Facility Level and Area Methane Emissions inventory for the Greater Toronto Area
 543 (FLAME-GTA). *Atmospheric Environment*, 252, p. 118319.
 544 <https://doi.org/10.1016/J.ATMOSENV.2021.118319>
- 545 Patton, E.G., Sullivan, P.P. and Davis, K.J. (2003). The influence of a forest canopy on top-down and bottom-up
 546 diffusion in the planetary boundary layer. *Quarterly Journal of the Royal Meteorological Society*,
 547 129(590), pp. 1415–1434. <https://doi.org/10.1256/QJ.01.175>
- 548 Peischl, J. *et al.* (2013). Quantifying sources of methane using light alkanes in the Los Angeles basin, California.
 549 *Journal of Geophysical Research: Atmospheres*, 118(10), pp. 4974–4990.
 550 <https://doi.org/10.1002/JGRD.50413>

- 551 Phillips, N.G. *et al.* (2013). Mapping urban pipeline leaks: Methane leaks across Boston,. *Environmental Pollution*,
552 173, pp. 1–4. <https://doi.org/10.1016/J.ENVPOL.2012.11.003>
- 553 Plant, G. *et al.* (2019). Large Fugitive Methane Emissions from Urban Centers Along the U.S. East Coast.
554 *Geophysical Research Letters*, 46(14), pp. 8500–8507. <https://doi.org/10.1029/2019GL082635>
- 555 Ren, X. *et al.* (2018). Methane Emissions from the Baltimore-Washington Area Based on Airborne Observations:
556 Comparison to Emissions Inventories. *Journal of Geophysical Research: Atmospheres*, 123(16), pp. 8869–
557 8882. <https://doi.org/10.1029/2018JD028851>
- 558 Sargent, M.R. *et al.* (2021). Majority of US urban natural gas emissions unaccounted for in inventories. *Proceedings*
559 *of the National Academy of Sciences of the United States of America*, 118(44).
560 <https://doi.org/10.1073/pnas.2105804118>
- 561 *Sixth Assessment Report — IPCC*. <https://www.ipcc.ch/assessment-report/ar6/> (Accessed: August 19, 2022).
- 562 Skamarock, W.C. *et al.* (2008). A description of the Advanced Research WRF version 3. NCAR Technical note -
563 475+STR. <http://130.203.136.95/viewdoc/summary?doi=10.1.1.484.3656> (Accessed: July 30, 2022).
- 564 Skamarock, W.C. and Klemp, J.B. (2008). A time-split nonhydrostatic atmospheric model for weather research and
565 forecasting applications. *Journal of Computational Physics*, 227(7), pp. 3465–3485.
566 <https://doi.org/10.1016/J.JCP.2007.01.037>
- 567 Turner, A.J. *et al.* (2016). A large increase in U.S. methane emissions over the past decade inferred from satellite
568 data and surface observations. *Geophysical Research Letters*, 43(5), pp. 2218–2224.
569 <https://doi.org/10.1002/2016GL067987>
- 570 *U.S. Census Bureau QuickFacts: United States*.
571 <https://www.census.gov/quickfacts/fact/table/arlingtoncountyvirginia,baltimorecitymaryland/SEX255221>
572 (Accessed: November 29, 2022).
- 573 Verhulst, K.R. *et al.* (2017). Carbon dioxide and methane measurements from the Los Angeles Megacity Carbon
574 Project - Part 1: Calibration, urban enhancements, and uncertainty estimates. *Atmospheric Chemistry and*
575 *Physics*, 17(13), pp. 8313–8341. <https://doi.org/10.5194/ACP-17-8313-2017>
- 576 Weil, J. C., & Horst, T. W. (1992). Footprint estimates for atmospheric flux measurements in the convective
577 boundary layer. *Precipitation Scavenging and Atmosphere-Surface Exchange*, 2, 717-728.
- 578 Weller, Z.D. *et al.* (2022). Environmental Injustices of Leaks from Urban Natural Gas Distribution Systems:
579 Patterns among and within 13 U.S. Metro Areas. *Environmental Science & Technology*, 56(12), 8599-
580 8609. <https://doi.org/10.1021/acs.est.2c00097>
- 581 Weller, Z.D., Hamburg, S.P. and von Fischer, J.C. (2020). A National Estimate of Methane Leakage from Pipeline
582 Mains in Natural Gas Local Distribution Systems. *Environmental Science and Technology*, 54(14), pp.
583 8958–8967. <https://doi.org/10.1021/acs.est.0c00437>
584 https://doi.org/10.1021/ACS.EST.0C00437/ASSET/IMAGES/LARGE/ES0C00437_0006.JPEG.
- 585 Welp, L.R. *et al.* (2013). Design and performance of a Nafion dryer for continuous operation at CO₂ and CH₄ air
586 monitoring sites. *Atmospheric Measurement Techniques*, 6(5), pp. 1217–1226.
587 <https://doi.org/10.5194/AMT-6-1217-2013>
- 588 Wunch, D. *et al.* (2009). Emissions of greenhouse gases from a North American megacity. *Geophysical Research*
589 *Letters*, 36(15). <https://doi.org/10.1029/2009GL039825>
- 590 Wyngaard, J.C. and Brost, R.A., 1984. Top-down and bottom-up diffusion of a scalar in the convective boundary
591 layer. *Journal of Atmospheric Sciences*, 41(1), pp.102-112.
592 [https://doi.org/10.1175/1520-0469\(1984\)041%3C0102:TDABUD%3E2.0.CO;2](https://doi.org/10.1175/1520-0469(1984)041%3C0102:TDABUD%3E2.0.CO;2)
- 593 Yadav, V. *et al.* (2019). Spatio-temporally Resolved Methane Fluxes from the Los Angeles Megacity. *Journal of*
594 *Geophysical Research: Atmospheres*, 124(9), pp. 5131–5148. <https://doi.org/10.1029/2018JD030062>
- 595 Yang, L. *et al.* (2018). A new generation of the United States National Land Cover Database: Requirements,
596 research priorities, design, and implementation strategies. *ISPRS Journal of Photogrammetry and Remote*
597 *Sensing*, 146, pp. 108–123. <https://doi.org/10.1016/J.ISPRSJPRS.2018.09.006>
- 598 Zimmerle, D.J. *et al.* (2015). Methane Emissions from the Natural Gas Transmission and Storage System in the
599 United States. *Environmental Science and Technology*, 49(15), pp. 9374–9383.
600 <https://doi.org/10.1021/acs.est.5b01669>

601

1 **Analysis of the trends in ambient methane in the Baltimore-Washington region and**
2 **comparison to model output**

3
4 *Sayantana Sahu¹, Anna Karion², Israel Lopez-Coto², Xinrong Ren³, Ross J. Salawitch^{1,4,5}, Russell R. Dickerson^{1,4,5}*

5
6 1. Department of Chemistry and Biochemistry, University of Maryland, College Park, Maryland, USA

7 2. National Institute of Standards and Technology, Gaithersburg, Maryland, USA

8 3. Air Resources Laboratory, National Oceanic and Atmospheric Administration, College Park, Maryland, USA

9 4. Department of Atmospheric and Oceanic Science, University of Maryland, College Park, Maryland, USA

10 5. Earth System Science Interdisciplinary Center, University of Maryland, College Park, Maryland, USA

11
12 Corresponding author: Sayantan Sahu ([sayantan@umd.edu](mailto:sayantana@umd.edu))

13
14 **Key Points:**

- 15
- 16 • Both versions of EDGAR (4.2 and 5.0) underestimate the regional anthropogenic emission of methane.
 - 17 • The correlation of modeled versus measured methane was stronger with the EDGAR
18 5.0.
 - 19 • Inclusion of fluxes of wetland emissions reduce the bias between modeled and
20 measured methane, especially in summer at the rural site.
- 21
22

23 **Abstract**

24 We studied atmospheric methane observations from November 2016 to October 2017 from one rural and two urban
25 towers in the Baltimore-Washington region (BWR). Methane observations at these three towers display distinct
26 seasonal and diurnal cycles with maxima at night and in the early morning, reflecting local emissions and boundary
27 layer dynamics. Peaks in winter concentrations and vertical gradients indicate strong local anthropogenic wintertime
28 methane sources in urban regions. In contrast, our analysis shows larger local emissions in summer at the rural site,
29 suggesting a dominant influence of wetland emissions. We compared observed enhancements (mole fractions above
30 the 5th percentile) to simulated methane enhancements using the WRF-STILT model driven by two EDGAR
31 inventories. When run with EDGAR 5.0, the low bias of modeled versus measured methane was greater (ratio of
32 1.9) than the bias found when using the EDGAR 4.2 emission inventory (ratio of 1.3). However, the correlation of
33 modeled versus measured methane was stronger (~1.2 times higher) for EDGAR 5.0 compared to results found
34 using EDGAR 4.2. In winter, the inclusion of wetland emissions using WETCHARTs had little impact on the mean
35 bias, but during summer, the low bias for all hours using EDGAR 5.0 improved by from 63 to 23 nanomoles per
36 mole of dry air or parts per billion (ppb) at the rural site. We conclude that both versions of EDGAR underestimate
37 the regional anthropogenic emissions of methane, but version 5.0 has a more accurate spatial representation.

38 **Plain Language Summary**

39
40 In this study we analyzed methane observations from three towers in the Baltimore-Washington region and used
41 these observations to evaluate anthropogenic and biogenic methane emission inventories. We found that
42 anthropogenic methane sources dominate at the urban sites while wetland emissions dominate at the rural site.
43 Significant discrepancies were observed between observations and methane outputs from a transport and dispersion
44 model run with different inventories, indicating substantially underestimated methane emissions in these inventories.
45 The low bias was greater with a newer version (EDGAR 5.0) than with an older version (EDGAR 4.2), however the
46 correlation was stronger with the newer version. We attribute the stronger correlation to improved spatial
47 distribution of methane emissions within the newer version. Adding wetland emissions reduced bias and improved
48 the seasonal cycle in modeled methane at the rural site.

49 **1. Introduction**

50 Methane is an important and not yet fully understood greenhouse gas, with a global warming potential of about 80
51 times more than carbon dioxide over a 20 year time horizon (Sixth Assessment Report — IPCC), although with an
52 atmospheric lifetime much shorter than carbon dioxide. There are both natural and anthropogenic sources of
53 methane. For example, natural sources include wetlands and wild animals while anthropogenic sources include the
54 production, transmission, distribution, and use of natural gas, as well as coal, livestock, wastewater treatment, and
55 landfills. In the United States (U.S.), natural gas and petroleum systems are the second largest source of methane
56 emissions after agriculture (Inventory of U.S. Greenhouse Gas Emissions and Sinks | U.S. EPA). Urban areas are a
57 significant source of anthropogenic methane emissions, often dominated by fugitive emissions from the natural gas
58 distribution and usage (Ren et al., 2018; Plant et al., 2019; Sargent et al., 2021).

59 Methane emissions from urban areas remain uncertain. Studies have attempted to assess and quantify the methane
60 emissions from natural gas leakage in urban centers and the transmission and storage (T&S) sector as a whole
61 (Alvarez et al., 2012, 2018; Peischl et al., 2013; Phillips et al., 2013; Jackson et al., 2014; Gallagher et al., 2015;
62 Kathryn et al., 2015; Lamb et al., 2015; Zimmerle et al., 2015; Hendrick et al., 2016; Cambaliza et al., 2017).
63 Substantial disparities exist between bottom-up estimates (inventories) and top-down estimates (based on
64 atmospheric measurements) with top-down estimates generally much larger than bottom-up values (Lamb et al.,
65 2016; Turner et al., 2016; Ren et al., 2018; Lopez-Coto et al., 2020). A recent study by Plant et al., (2019) used
66 aircraft measurements to conclude that methane emissions from many urban centers along the U.S. East Coast are
67 more than twice those in inventories. Ren et al., (2018) and Lopez-Coto et al., (2020) used airborne measurements to
68 determine that the winter (February) methane emission rates in 2016 in the Baltimore-Washington region (BWR)
69 were 2.7 to 2.8 times the US national greenhouse gas inventory for 2012. Huang et al., (2019), used atmospheric
70 inversions with methane observations from towers in the BWR and found methane emissions underestimated by the
71 existing inventories in fall, winter, and spring but overestimated in summer because of excess modeled wetland
72 emissions.

73 Few studies have looked at how models reproduce observed diurnal and seasonal trends of methane. Yadav et al.,
74 (2019) and He et al., (2019) used continuous observations (tower-based and remote-sensing, respectively) in the
75 Southern California air basin to show seasonality in urban methane emissions. Sargent et al., (2021) showed distinct
76 seasonality in methane emissions in Boston using in-situ observations in that city as well. Huang et al., (2019) used
77 data from afternoon hours (12 pm to 5 pm) and discovered a significant seasonality in urban methane emissions in
78 the BWR. The objective of our study is to evaluate anthropogenic and biogenic methane emission inventories with
79 ambient observations from towers. The aim is to better understand the sources and to evaluate existing inventories of
80 methane. We studied in-situ methane data from the BWR under the Northeast Corridor (NEC) project using two
81 urban towers ARL (Arlington, VA), NEB (Northeast Baltimore, MD), and one rural tower, BUC (Bucktown, MD)
82 (Karion et al., 2020). Karion et al., (2020) discussed methane measurements from two of these three towers – ARL
83 and BUC. The methane observations from these towers displayed distinct seasonal and diurnal cycles with seasonal
84 maxima in winter at the urban towers reflecting greater emissions and reduced vertical mixing, and larger vertical
85 gradients at night and early morning, indicating significant local emissions and higher concentrations when the
86 planetary boundary layer (PBL) is shallow. At BUC, the rural site, Karion et al., (2020) observed large vertical
87 gradients during the early morning hours in the summer, suggesting substantial local wetland emissions expected to
88 peak when the surface is warm. In our study, we compared modeled methane enhancements to observed
89 enhancements. We used the meteorological WRF (Weather Research and Forecasting) Model (Skamarock et al.,
90 2008) in combination with Lagrangian dispersion model STILT (Stochastic Time-Inverted Lagrangian Transport
91 model) (Lin et al., 2003; Nehr Korn et al., 2010) to simulate time series of methane at each tower location. We

92 compared the tower methane observations with the model outputs and used the ambient observations to evaluate the
93 anthropogenic and biogenic methane emission inventories.

94 **2. Methods**

95 **2.1. Tower locations and observations**

96 The NEC tower network, currently consisting of 29 stations, was initiated in 2015, with the primary objective to
97 better quantify urban emissions of anthropogenic greenhouse gases (Karion et al., 2020). Sixteen stations were
98 established around the BWR to estimate greenhouse gas emissions using inverse modeling techniques (Lopez-Coto
99 et al., 2017; Mueller et al., 2018). The tower network design and location under NEC, data collection, processing,
100 instrumentation, and calibration have been discussed in detail in earlier publications (Welp et al., 2013; Verhulst et
101 al., 2017; Lopez-Coto et al., 2017; Mueller et al., 2018; Karion et al., 2020). We used continuous, hourly
102 measurements of methane from the three towers in the region - NEB, ARL, and BUC. NEB is located in the city of
103 Baltimore, where the median household income is \$52,164, while ARL is in Arlington, VA, a moderately developed
104 suburb of Washington DC with over twice the median income of Baltimore (\$122,604) (U.S. Census Bureau). Both
105 are classified as urban towers (Karion et al., 2020). BUC is located in Bucktown, MD, on the eastern side of
106 Chesapeake Bay, in a wetland-dominant region (Karion et al., 2020). The location of these towers and the sampling
107 heights are provided in Table S1 & Figure S1, and also in Huang et al., (2019) and Karion et al., (2020).

108 We analyzed the diurnal and seasonal variation of methane at these three towers using contour plots as
109 previously done in Bloomer et al. (2010). We computed the hourly averages of the methane observations for each
110 month to generate these plots. We used data for the period November 2016 to October 2017 and focused our model
111 comparison analysis in two ecological seasons - winter (December 2016 to February 2017) and summer (June to
112 August 2017). Our research considered data from the entire diurnal cycle to determine how effectively the model
113 run with various inventories can replicate the observed diurnal trends. We used results from only the lower sampling
114 height (46m to 50 m above ground level) for the model bias comparison but obtained similar results when
115 considering data from the upper sampling height. Data from both sampling heights of each tower were used for the
116 vertical gradient analysis.

117

118 **2.2. Description of model and inventories**

119 Our study used the STILT transport and dispersion model (Lin et al., 2003b) run with meteorological data from
120 WRF model (Skamarock and Klemp, 2008; Skamarock et al., 2008) and configured as described in (Karion et al.,
121 2021). STILT was run 120 h backward in time from the observation points – the locations of the towers in our study.
122 The surface influence (proportional to the residence time of a particle over a given pixel and within the planetary
123 boundary layer) for each observation, or footprint, was calculated. The surface influence at each pixel was
124 multiplied by the emissions inventory's surface flux ($\mu\text{mol}/\text{m}^2/\text{s}$). The sum over all pixels equals the modeled mole
125 fraction enhancement at the tower site. Footprints were generated for each tower for a regional domain (bounds 92.0
126 W, 68.0 W, 33.0 N, 47.0 N) at 0.1-degree resolution. The domain is shown in Figure S2.

127 We used two anthropogenic CH₄ emission inventories – the Emission Database for Global Atmospheric Research
128 versions 4.2 (hereafter referred to as EDGAR 4.2) (Janssens-Maenhout et al., 2013) and 5.0 (hereafter referred to as
129 EDGAR 5.0) (EDGAR - Joint Research Centre Data Catalogue - EDGAR v5.0 Greenhouse Gas Emissions -
130 European Commission; Crippa et al., 2019) for 2012. The inventories have a horizontal resolution of 0.1° latitude by
131 0.1° longitude. There is no seasonality in methane emissions in EDGAR 4.2 and essentially no variation (< 5%) with
132 season in EDGAR 5.0 in our model domain or near our towers. Here, we used the annual average of emissions for a
133 particular year in the model. We chose these two versions of EDGAR because they have the most different spatial
134 representation of emissions, with EDGAR 4.2 placing more emissions in urban centers (i.e., emissions are
135 downscaled via population) than EDGAR 5.0. (Janssens-Maenhout et al., 2013). The distribution of methane
136 emissions within the inventories for the area near the towers is discussed in the results section.

137

138 **2.3. Comparison of observations and model outputs**

139 Our study considered several methods to compare modeled wetland emissions with observations. To
140 account for wetland methane emissions, we used wetland fluxes derived from WetCHARTs, with a horizontal
141 resolution of 0.5° latitude by 0.5° longitude (Bloom et al., 2017). WetCHARTs consists of 18 emission models, of
142 which nine exhibit higher magnitude of methane wetland fluxes than others, while the remaining 9 models are
143 significantly lower in magnitude and have different spatial allocations of wetland emissions (Figures S3a-b). We
144 calculated the mean from the 9 models with higher magnitude (hereafter referred to as ‘wet 3a’) and lower
145 magnitude (hereafter referred to as ‘wet 4a’) of wetland fluxes averaged monthly over 15 years. We also determined
146 the mean of all 18 models over 15 years (hereafter referred to as ‘wet ma’) for comparison with observations. In
147 addition to the three scenarios mentioned above (wet 3a, wet 4a and wet ma), we have downscaled the emissions to
148 our 0.1° model resolution using the wetland fraction (calculated as the sum of woody and herbaceous wetlands) from
149 the National Land Cover Database (NLCD) 2016 (Yang et al., 2018), conserving the mass within each 0.5° cell. We
150 have referred to the scenarios as ‘wet 3b’, ‘wet4b’, and ‘wet mb’.

151 We adopted a simple approach to directly compare the model outputs with methane tower observations.
152 The WRF-STILT model footprints are convolved (multiplied pixel by pixel and then summed) with inventories
153 (both anthropogenic and WetCHARTs) to simulate methane mole fraction enhancement in nanomoles of methane
154 per mole of dry air, (nmol mol⁻¹), or parts per billion (ppb), interpreted as excess methane over the atmospheric
155 background concentration. Due to the small number of towers used in this work and the fact that none of them could
156 really be considered a background tower, we decided to apply a simplified background methodology, treating each
157 tower independently, as opposed to more complex background methods as described in Karion et al., (2021). We
158 subtracted the 5th percentile, similarly to Pak et al., (2021) but determined seasonally for each tower, from the
159 absolute methane mole fractions from both the tower observations and the modeled output. We repeated our analysis
160 with the 2nd, 10th, and 15th percentile (Tables S2-3) subtracted from the methane tower observations and the model
161 results and found that while the choice of percentile impacts the magnitude of the biases it did not impact the
162 direction of the biases, the normalized mean bias (see below), nor the general conclusions; here, we presented results
163 using the 5th percentile.

164 We added the WetCHARTs modeled outputs to the EDGAR outputs (and subsequently deducted the 5th
 165 percentile) to determine if the inclusion of wetland emissions could bring better agreement between the model and
 166 observations. We used the bias and normalized mean bias (hereafter referred to as NMB) of methane to quantify the
 167 discrepancies between the model and observations. The NMB gives a good idea of how significant the bias is
 168 relative to the signal (enhancement). The two quantities were calculated as follows,

169

$$170 \quad \text{Mean bias (ppb methane)} = \frac{\sum_{i=1}^n (\text{model}_i - \text{obs}_i)}{n}$$

171 (Eq. 1)

172

$$173 \quad \text{Normalized mean bias (NMB)} = \frac{\sum_{i=1}^n (\text{model}_i - \text{obs}_i)}{\sum_{i=1}^n \text{obs}_i}$$

174 (Eq. 2)

175

176 (n = number of observations)

177

178 Here, ‘obs’ and ‘model’ refer to the observations and modeled output above the 5th percentile. A negative mean bias
 179 will be reflective of the model underestimating observations. We also calculated the least squares coefficient of
 180 determination (r^2) between methane observations and the model.

181 We investigated the methane vertical gradients between the two inlet heights at the three towers and
 182 compared these with model output. The analysis of vertical gradients will help understand whether the towers are
 183 located in the vicinity of sources (Monteiro et al., 2022). When the PBL is not well-mixed (e.g., at night or early
 184 morning), ground-level emissions near the tower result in higher concentrations at the lower level, thus larger
 185 gradients indicate higher emissions near the tower.

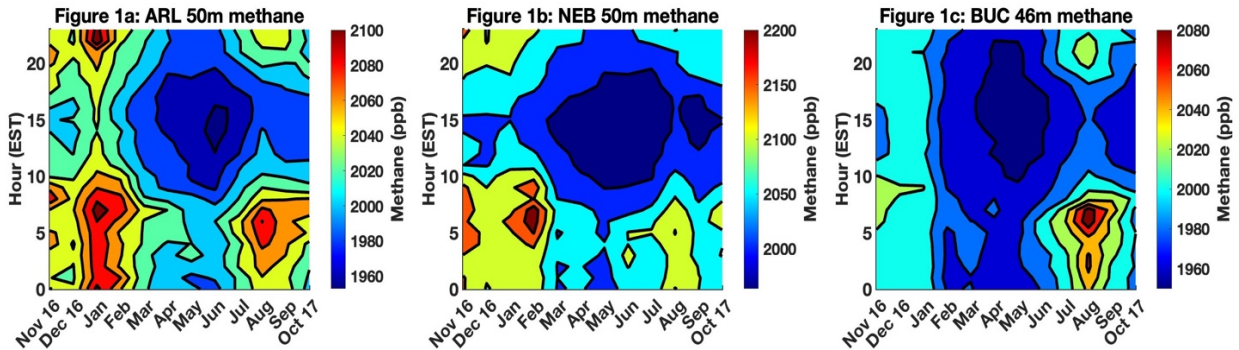
186 **3. Results**

187 **3.1. Analysis of methane observations at the three towers**

188 Methane measurements from the three towers in our study display distinct diurnal and seasonal cycles with daily
 189 maxima in the early morning and night hours (Figure 1). The presence of such distinct early morning and nighttime
 190 local maxima indicates local emissions. These maxima can be explained by the buildup from local emissions in the
 191 shallower boundary layer that are later dissipated due to turbulent mixing in the afternoon hours. The methane
 192 contour plots at the urban sites, NEB and ARL, show that this early morning enhancement is greatest during winter,
 193 but a secondary maximum in the early morning also appears in the late summer months (around August). The higher
 194 ambient concentration in the early morning and night hours in winter can be attributed to both enhanced
 195 anthropogenic methane emissions in winter and to the seasonality of boundary layer heights (Huang et al., 2019;
 196 Karion et al., 2020). Minima are observed in the summer afternoons when the PBL is deepest. The pattern indicates
 197 the importance of local emissions in the vicinity of the tower. The urban sites show a dominant winter peak
 198 suggesting that leakage from the natural gas (NG) system may be a major local source, if NG system emissions are

199 higher in winter than summer, as suggested by previous urban studies (He et al., 2019; Sargent et al., 2021). The
 200 secondary summer peak indicates that other, likely biogenic, sources may also be at play. Seasonality in
 201 meteorological conditions, including the PBL, also plays a role.

202



203

204

205 **Figure 1.** Methane contour plots showing diurnal and seasonal variation of methane at the three towers for the
 206 period November 2016 – October 2017. The data are from the lower inlet height of the towers 50 m above ground
 207 level for NEB and ARL and 46 m for BUC. Note the color bars are different in each plot.

208

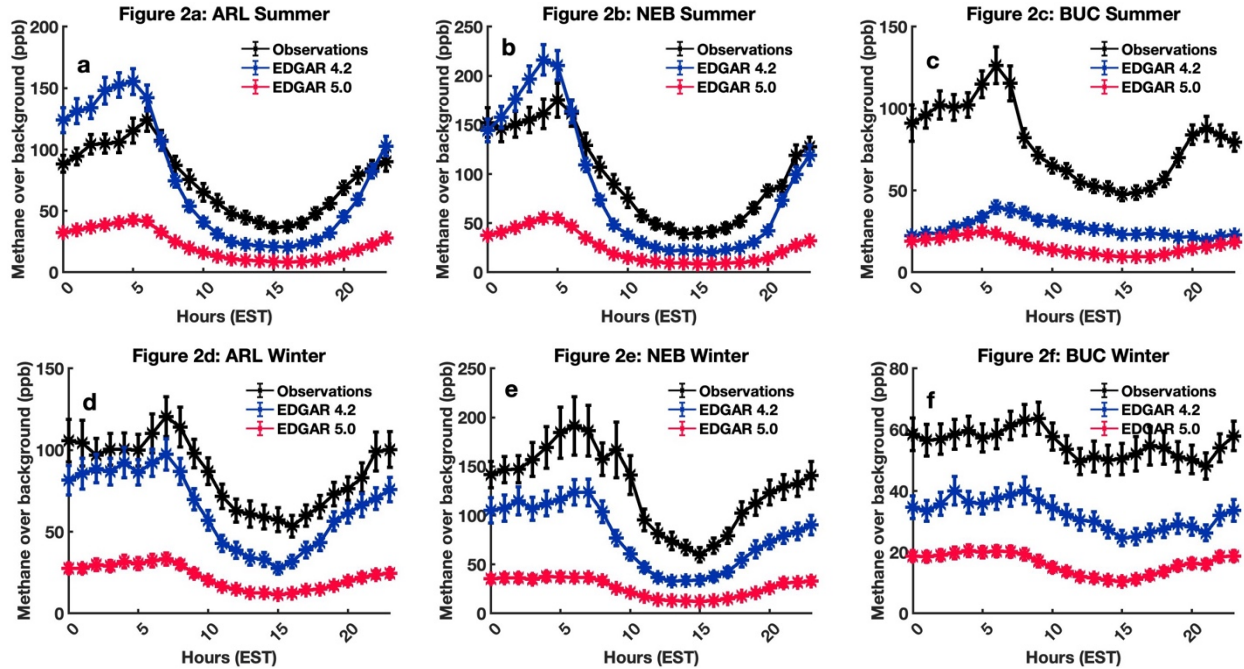
209 Unlike the urban sites, the rural BUC site shows a dominant early morning enhancement during the summer months,
 210 indicating a strong local biogenic process more pronounced at higher temperatures. This late summer maximum is
 211 coincident with the summer maxima discussed for the urban towers (ARL and NEB), indicating that these towers
 212 might also be impacted by biogenic sources. BUC is located in Dorchester County, MD, with close to 68,400
 213 hectares of estuarine and palustrine wetlands, besides agricultural land. This site shows a minor winter maximum
 214 likely related to PBL dynamics coupled with some minor emissions in winter. The absolute values of the methane
 215 mole fractions are greatest at NEB and smallest at BUC. These patterns suggest that urban methane emissions are
 216 greater than rural emissions in the BWR.

217

218 3.2. Comparison of observed and modeled diurnal cycles of methane

219 We analyzed both the observed and modeled diurnal variations of methane enhancements at all three towers to
 220 investigate how accurately the models captured the observed diurnal trends of methane. The modeled outputs were
 221 derived from the WRF-STILT runs with the EDGAR inventories as described in the Methods section. The plots in
 222 Figures 2a-f show the observed diurnal cycles of methane enhancements plotted along with the WRF-STILT model
 223 predicted diurnal cycles, run with EDGAR 4.2 or EDGAR 5.0.

224



225

226

227

228 **Figure 2.** Diurnal cycles of methane enhancements during summer (a-c) and winter months (d-f) at two urban
 229 towers, ARL and NEB, and one rural tower, BUC. The black line represents the hourly averaged methane
 230 observations; the blue and red lines represent modeled diurnal trends run with EDGAR 4.2 and EDGAR 5.0
 231 inventories respectively using the 5th percentile as background. The error bars represent the standard error of the
 232 mean, i.e., the standard deviation of the hourly observations divided by the square root of the number of
 233 observations used to calculate the mean.

234

235 3.2.1. Analysis of observed diurnal cycles of methane

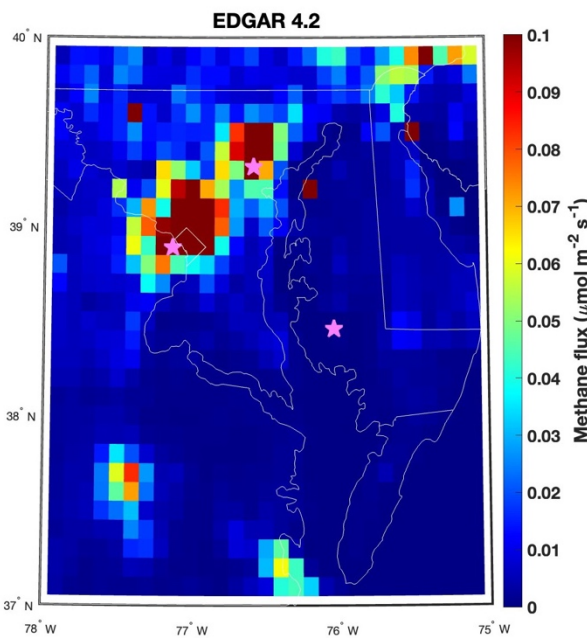
236 The observed diurnal cycles of methane enhancements for the three sites displayed a pronounced maximum in the
 237 early morning and the night, as also shown in Figure 1 and suggesting local emissions. As explained earlier, local
 238 emissions produce maxima in concentrations when the PBL is shallow. At the two urban sites, the magnitude of
 239 observed early morning maximum was greater during the winter than the summer. A plausible reason could be
 240 greater local anthropogenic methane emissions during winter due to increased NG use for heating, resulting in a
 241 higher early morning maximum in the diurnal cycle (He et al., 2019; Sargent et al., 2021), but also possibly caused
 242 by lower mixing layer depths in winter compared to summer. At BUC, a prominent diurnal cycle was seen during
 243 summer with a weaker variation during winter, suggesting that it is influenced by strong summer-time local sources,
 244 while winter-time enhancements originated farther from the tower, or by weak, local sources. Figure 1b shows
 245 evidence of strong seasonal emissions, likely from wetlands, at BUC that may explain the diurnal cycle in summer
 246 and near absence of it in winter.

247

248 3.2.2. Analysis of modeled diurnal cycles of methane to determine model - observation bias

249 It is evident from Figures 2a-f that significant discrepancies exist between the modeled and observed enhancements
 250 at all three towers. The WRF-STILT runs with both EDGAR inventories underestimate the enhancement of methane
 251 substantially in most cases at all three sites. EDGAR does not include wetland emissions of methane, which can
 252 plausibly explain the discrepancies between model and methane observations, especially in summer. WRF-STILT
 253 driven with the EDGAR 5.0 inventory has a greater negative bias relative to methane observations than when driven
 254 with EDGAR 4.2. In general, the EDGAR 4.2 inventory appears to reproduce the observed diurnal trend better (with
 255 less bias) than EDGAR 5.0.

256 In the winter, both EDGAR inventories underestimate methane during all hours, at all three towers. This is
 257 clear evidence of the model underestimating anthropogenic methane emissions, as we do not expect large natural
 258 emissions from wetlands in winter. The bias is greater with EDGAR 5.0 than with EDGAR 4.2, however. The
 259 spatial distributions of methane emissions within the area near the towers for both EDGAR 4.2 and EDGAR 5.0 are
 260 shown in Figures 3a-b. The total methane emissions within this area are significantly higher in EDGAR 4.2 (a factor
 261 of 1.85 in the area shown in Figure 3) compared to EDGAR 5.0. In addition, EDGAR 4.2 has more concentrated
 262 emissions around the cities, which strongly influence observations at the urban sites. These factors combined result
 263 in higher modeled enhancements relative to EDGAR 5.0 and thus lower bias. Both EDGAR inventories
 264 underestimate observed methane enhancements at BUC during winter, when wetland emissions are minimal,
 265 suggesting that these inventories also underestimate anthropogenic methane emissions upwind of this rural site. The
 266 bias is lower, in absolute magnitude, during the afternoon hours, when the boundary layer is well mixed, than at
 267 other times of the day, but still substantial.
 268



269
270
271
Figure 3a

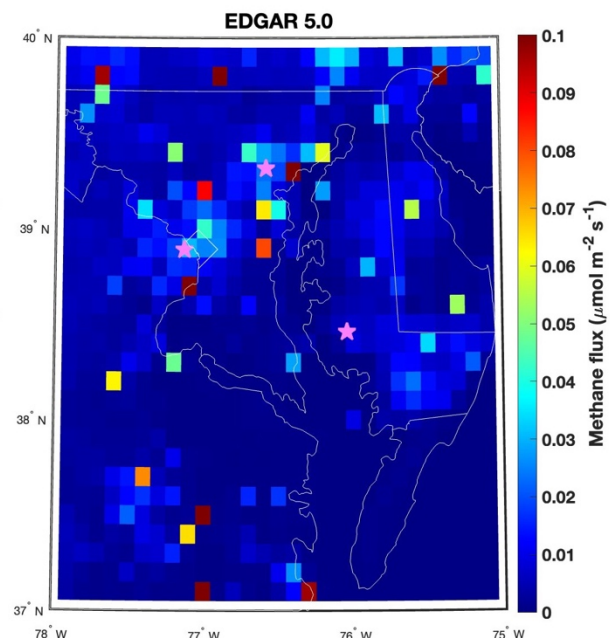


Figure 3b

272 **Figures 3.** Distribution of CH₄ emission fluxes (in units of $\mu\text{mol}/\text{m}^2/\text{s}$) in EDGAR 4.2 (left) and EDGAR 5.0 (right)
 273 around the towers used in our analysis. The pink stars represent the towers in our study. Color axis has been
 274 truncated for clarity.

275
 276 At the urban towers during the summer months, EDGAR 5.0 underestimates methane observed enhancements at all
 277 hours. However, EDGAR 4.2 underestimates methane enhancements during afternoon hours but overestimates them
 278 during early morning hours. A plausible explanation of the overestimation could be lower emissions of methane
 279 during summer compared to winter (Huang et al., 2019), combined with potential inaccurate representation of
 280 planetary boundary layer dynamics in the transport model. Emissions of methane within EDGAR versions used here
 281 are averaged annually, so there is no temporal variability in the anthropogenic emissions used in the model. During
 282 the summer months at BUC, the rural site in an area of extensive estuaries and other wetlands, significant
 283 discrepancies between the modeled and observed enhancements exist at all hours. This can be explained by the fact
 284 that EDGAR inventories do not include natural (wetland) emissions, discussed below.

285

286 3.2.3. Mean bias, NMB, correlation between observed and modeled methane enhancements

287 To quantify the bias between model outputs and observed methane enhancements, we analyzed the mean bias (Eq.
 288 1), normalized mean bias (NMB, Eq. 2), and the coefficient of determination (r^2). The results for summer and winter
 289 afternoon hours (12 pm to 3 pm EST) are tabulated in Table 1 and all hours in Table S4.

290

291

292 **Table 1**

293 *Mean bias (in ppb of methane, i.e., nmol/mol), normalized mean bias, and r^2 between modeled and observed*
 294 *enhancements for winter and summer afternoon hours, using the 5th percentile background.*

295

Tower	Inventory	Season	Mean bias (ppb)	NMB	r^2
BUC	EDGAR 4.2	winter	-22.26	-0.44	0.26
NEB		winter	-42.50	-0.52	0.38
ARL		winter	-26.97	-0.40	0.33
BUC	EDGAR 5.0	winter	-37.50	-0.74	0.29
NEB		winter	-65.93	-0.80	0.39
ARL		winter	-51.78	-0.77	0.36
BUC	EDGAR 4.2	summer	-35.10	-0.60	0.30
NEB		summer	-26.98	-0.49	0.18
ARL		summer	-18.78	-0.39	0.28
BUC		summer	-46.38	-0.80	0.36

NEB	EDGAR 5.0	summer	-43.39	-0.79	0.22
ARL		summer	-36.40	-0.75	0.36

296

297 *Note.* The corresponding table for all hours is in Table S4.

298

299 On average, the modeled methane enhancements are biased low in winter by approximately 22 ppb to 37 ppb at
300 BUC, and by 27 ppb to 66 ppb for the urban towers (NEB and ARL), depending on which EDGAR inventory is
301 used. The bias is greater for the urban towers compared with the rural site, and greater with EDGAR 5.0 than with
302 4.2 at all sites. During summer, the low bias ranges from approximately 19 ppb to 46 ppb when considering the three
303 towers. There is a greater low bias at the urban towers (NEB and ARL) during winter than at BUC. Conversely
304 during summer, the model low bias was greater at BUC than at the two urban towers. We attribute these tendencies
305 to weak wetland emissions during winter at the rural site that are amplified during summer. The urban towers are
306 influenced by the local anthropogenic methane emissions, likely from the NG distribution system or end usage,
307 which recent studies have suggested are higher in winter (He et al., 2019; Huang et al., 2019; Sargent et al., 2021).
308 Moreover, during winter, local emissions have a greater impact on observed enhancements due to the shallower
309 boundary layer. We arrive at the same conclusions when considering all hours of the day (Table S4). The low bias is
310 reduced to 1 ppb to 10 ppb of methane at the urban towers during summer when using EDGAR 4.2 due to the
311 overestimation by the model at early morning hours (Figures 2a-b). The bias is the smallest when only afternoon
312 hours are considered, possibly due to the smaller overall enhancements and because the transport model may
313 perform better under well-mixed conditions.

314 We compare the coefficient of determination (r^2) between modeled and observed CH₄ enhancements within
315 each season. Modeled methane from EDGAR 5.0 correlates better with observations than EDGAR 4.2 in most cases
316 despite the greater low bias, likely due to the improved spatial distribution of methane emissions in the newer
317 version. However, while EDGAR 5.0 correlates better with observations, it has a greater negative bias because it has
318 lower emissions, especially around urban centers. We note here that although a newer version of EDGAR (6.0) is
319 now available, it is very similar in both magnitude and spatial distribution to EDGAR 5.0 (Figure S4), so we would
320 not expect its use to yield any significant difference in our results.

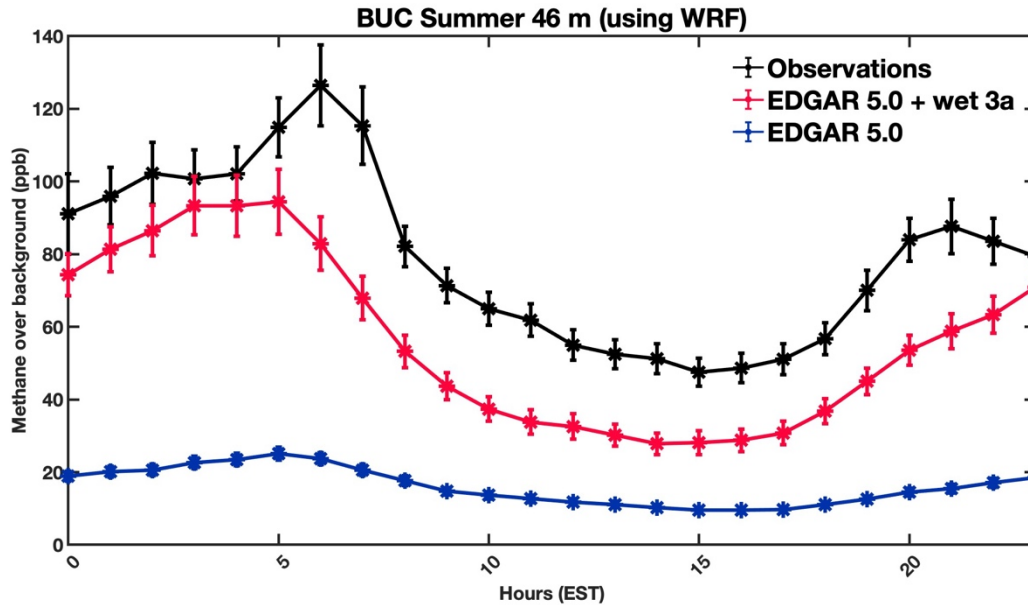
321

322 3.3. Incorporating wetland emissions using WETCHARTs

323 The summer concentration peak at BUC (an area of extensive estuaries and other wetlands) suggests strong natural
324 flux from wetlands, which are not included in the EDGAR anthropogenic emissions inventory. We thus ran the
325 model with WetCHARTs version 1.3.1 and added the resulting modeled enhancements from wetland emissions to
326 the anthropogenic enhancements from EDGAR 5.0 (See Figure 4, S5a-b and Tables S7-10). We used WRF-STILT
327 outputs with EDGAR 5.0 rather than 4.2 as EDGAR 5.0 better correlated with observations. Our findings suggest
328 that during winter, the addition of various WetCHARTs combinations has little impact on the bias, as expected
329 (wetland emissions are very small in winter (Figure S3)). The combinations ‘wet 3a’ and ‘wet 3b’ produce the
330 smallest bias under all scenarios, as these include the WetCHARTs members that have significantly higher methane

331 flux than others. During winter afternoon hours, the model was still biased low by approximately 35 ppb, 63 ppb, 50
 332 ppb at BUC, NEB, and ARL, respectively. The continued underestimation by the model during winter after
 333 incorporating wetland emissions is clear evidence of EDGAR 5.0 underestimating anthropogenic emissions of
 334 methane in this region.

335



336

337

338 **Figure 4:** Diurnal cycle of methane at BUC during summer. The black line represents the hourly averaged methane
 339 observations. The red and blue lines represent the model predicted diurnal trends using the EDGAR 5.0 inventory,
 340 with and without wetland emissions, respectively. The error bars represent the standard error of the mean of the data
 341 in hourly bins.

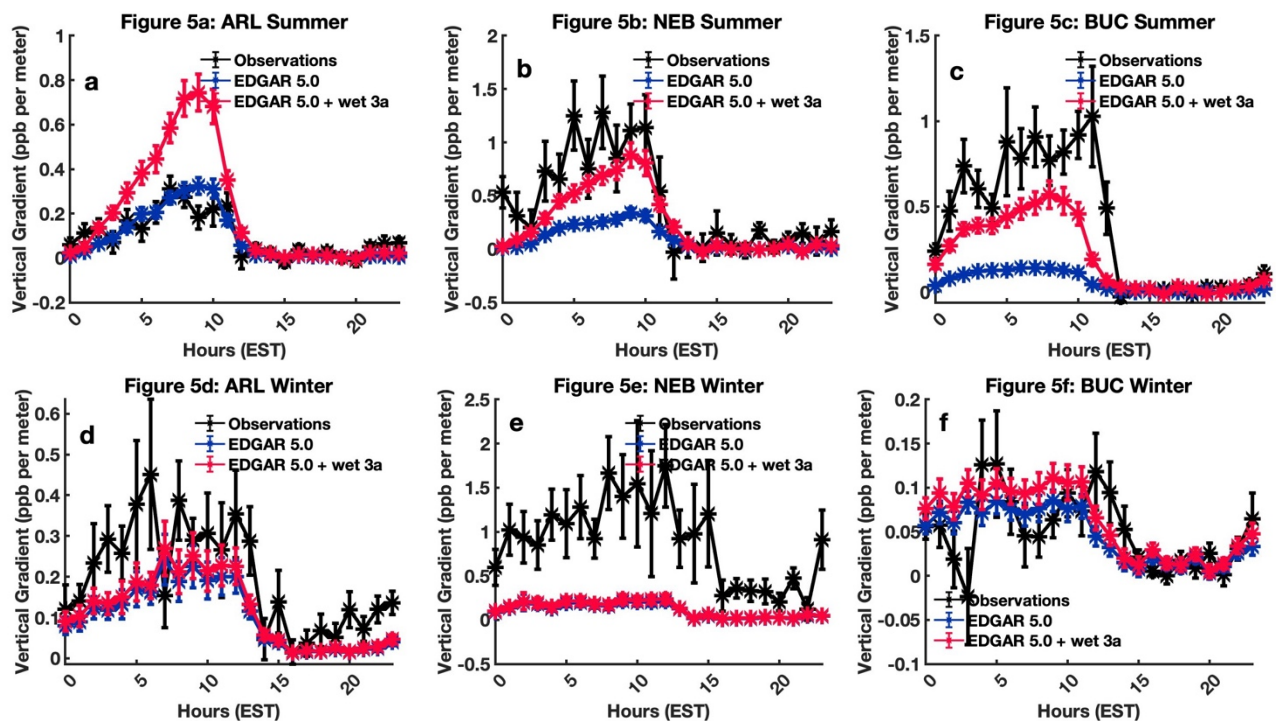
342

343 In summer, we observe much better agreement between modeled and observed CH₄ enhancements after including
 344 the effect of wetland emissions in the model. The negative model bias falls to approximately 20 ppb during
 345 afternoon hours at the three towers and ranges from approximately 12 to 28 ppb when considering all hours. Thus,
 346 even after adding wetland emissions in summer, a substantial bias remains, suggesting that WetCHARTs either
 347 underestimates the magnitude of wetland emissions or that the anthropogenic underestimation is so large that it is
 348 not compensated for by including wetland emissions. Adding WetCHARTs improves the seasonal cycle in modeled
 349 CH₄ at BUC as the summer afternoon low bias improves from approximately 46 ppb to 20 ppb. We compare the
 350 correlation (Tables S7-10) for the summer and winter seasons after adding modeled methane enhancements from
 351 WetCHARTs and find no improvement. The above observations show that WetCHARTs can be improved in both
 352 magnitude and spatial allocation of wetland emissions of methane.

353

354 **3.4. Analysis of observed and modeled Vertical gradient of methane**

355 We compared the observed and modeled vertical gradient of methane at the three towers for the winter and summer
 356 months. The vertical gradient was calculated as the difference in methane observations between the lower and the
 357 upper height, divided by the difference in inlet heights. A weak vertical gradient is indicative of a better mixed
 358 boundary layer or absence of strong local sources and sinks. When the boundary layer is not well-mixed, the
 359 gradient shows if there are local sources. The vertical gradient can help us better understand if strong local sources
 360 of methane influence the tower observations (Wyngaard et al., 1984; Dyer, 1974; Patton, Sullivan and Davis, 2003;
 361 Monteiro et al., 2022). However, the difference between modeled and observed vertical gradients is a function of
 362 both the accuracy of the emissions used in the model and the ability of the transport and dispersion model to
 363 simulate vertical mixing accurately. Figure 5 shows the diurnal variations of the observed and modeled vertical
 364 gradients at the three towers in summer (Figures 5a-c) and winter (Figures 5d-f).
 365



366

367

368

369 **Figure 5.** Vertical gradients of methane at the three towers in summer (a-c) and in winter (d-f). The black lines
 370 represent observed vertical gradient between the two inlet heights at the towers. The blue and the red lines represent
 371 the model simulated vertical gradient without wetland emissions and with ‘wet 3a’ emissions from WetCHARTs,
 372 respectively. The error bars represent the standard error of mean of vertical gradients in hourly bins.

373

374 3.4.1. Observed Vertical gradient of methane

375 We observe a large vertical gradient at both urban towers in the early morning hours that plummets in the afternoon
 376 hours (consistent with the early morning concentration maximum seen in Figure 1). The strong vertical gradient in
 377 the morning hours indicates that the towers are situated in the vicinity of methane sources. The pattern is similar
 378 during winter and summer; however, the morning vertical gradient is slightly higher during winter, which can be

379 attributed either to the seasonality of the nocturnal vertical mixing or greater anthropogenic methane emissions
380 during winter or both. In contrast, at BUC, we observe strong vertical gradients during summer, but they are close to
381 zero during winter indicating that local sources during this season are very weak. The strong summer vertical
382 gradients can be explained by local wetland emissions influencing observations at this site, and the bulk of
383 anthropogenic sources being farther away.

384

385 **3.4.2. Modeled Vertical gradient of methane**

386 We analyzed how reliably WRF-STILT run with EDGAR 5.0 can reproduce the observed vertical gradients at the
387 three towers. We included modeled methane enhancements from WetCHARTs “3a” (the mean of the high-emission
388 members) to account for biogenic emissions, because the “3a” version better matched summer observations at BUC
389 in our previous analysis. The discrepancy between observed and modeled vertical gradients at all three sites is
390 lowest during the late afternoon hours when the boundary layer is well-mixed. The results are congruent with the
391 results in the previous section, where we compared the observed and model-simulated diurnal patterns of methane
392 enhancements. At NEB and ARL, the inclusion of wetland emissions during winter does not substantially improve
393 the model bias, as they are very small in winter (see Tables S7-8). At ARL, during winter, we observed good
394 agreement between model outputs and observations, with a bias of approximately 0.1 ppb per meter during early
395 morning hours and less than 0.1 ppb per meter during the afternoon. At NEB, the model was biased low by
396 approximately 1 ppb per meter in the early morning hours and approximately 0.2 ppb per meter during the afternoon
397 hours, most likely due to local sources being underestimated in EDGAR 5.0.

398 During summer, at ARL, the model run with EDGAR 5.0 reproduces the observed diurnal trend in vertical
399 gradient remarkably well; however, the inclusion of wetland emissions overestimates the early morning gradient. In
400 contrast, at NEB during summer, the model simulations with the addition of wetland emissions significantly reduce
401 the bias between the modeled and observed vertical gradient, from approximately 1 to 0.2 ppb per meter. Thus,
402 either wetland emissions are influencing observations at NEB in summer, or (more likely, given the lack of nearby
403 wetlands) the additional modeled emissions are compensating for the large under-estimation of anthropogenic
404 emissions in EDGAR 5.0 at this site. At BUC, during winter, in the absence of any strong local sources, we observe
405 good agreement between model outputs and observations at all hours. During summer, when wetland emissions are
406 greatest, the addition of WetCHARTs output in the model significantly reduces the bias, especially during morning
407 hours, when local emissions are most significant.

408

409 **3.5. Contrasting urban sites - NEB and ARL**

410 When we compare the methane diurnal cycle at the two urban towers, we find greater methane enhancements at
411 NEB when compared to ARL. The absolute methane mole fractions are also greater at NEB than ARL (Figures 1a-
412 b). This may be the result of ARL being generally more upwind of the BWR and NEB being more generally
413 downwind, or to greater emissions near NEB, possibly due to fugitive methane emissions from leaks in the delivery
414 system (Weller, Hamburg and von Fischer, 2020). In this paper, we have pointed out the potential impact of natural
415 gas on observations, but local sources could also be from urban wastewater treatment and landfills.

416 Demographics and infrastructure may play a role in the differences of methane concentrations at the two
417 sites. The observation raises a pertinent question of environmental justice (Weller et al., 2022), as methane
418 concentrations may correlate with higher concentrations of other pollutants that affect health outcomes; future
419 studies should further investigate differences in methane sources and emissions magnitudes in these two cities
420 (Arlington, VA and Baltimore, MD). When comparing observations to modeled enhancements, we discover more
421 extreme bias toward low values in the model for the NEB than ARL (NMB 0.80 vs 0.77 for winter afternoon with
422 EDGAR 5.0), see Table 1. The difference can be because EDGAR 5.0 emissions are too low near NEB but more
423 accurate near ARL, compared to observed data, as also suggested by the vertical gradients.

424 **5. Conclusions**

425 Our study compared methane observations from three towers with output from a Lagrangian model using diurnal
426 patterns and vertical gradients. Results suggest that anthropogenic methane emissions dominate in the urban areas
427 (sites NEB and ARL) while natural (i.e., wetland) sources dominate at the rural site (BUC). Significant
428 discrepancies were found between models driven by EDGAR and observations; while EDGAR 5.0 seems to have an
429 improved spatial distribution of emissions (as suggested by higher correlations with observed enhancements), its
430 emissions magnitude in these two cities is too low. EDGAR 4.2, with larger urban emissions, compared more
431 favorably with observations in terms of magnitude. Both daily cycle and vertical gradient comparisons point toward
432 higher local emissions near NEB relative to ARL and higher emissions during winter than in summer at these urban
433 sites, although more work is needed to confidently conclude this. In addition, adding wetland emissions from
434 WetCHARTs significantly improved the agreement between modeled and observed vertical gradients especially in
435 summer at BUC. While adding wetland emissions from WetCHARTs reduced discrepancies in terms of bias,
436 especially in summer, the lower correlation observed might indicate that the distribution of these emissions could
437 still be improved and that we need better wetland models with greater resolution to replicate observations from the
438 mid-Atlantic wetland region. Besides the known anthropogenic emissions, we found evidence of additional summer
439 (possibly biogenic) emissions at the urban sites based upon analyses of the seasonal and temporal patterns of
440 observed methane. Future studies should investigate the source of summertime emissions around these sites and the
441 strength of these sources relative to the anthropogenic source of methane. We note that here we have investigated
442 CH₄ observations near towers using a simple seasonal background; a more quantitative determination of CH₄
443 emissions would require a more sophisticated treatment of background (e.g., Karion et al., 2021) and likely a higher
444 resolution modeling framework. Finally, future measurements of ethane and ¹³C isotopic analysis along with
445 methane might help distinguish the relative strength of biogenic and anthropogenic sources.

446 **Acknowledgments and Data Availability**

447 The authors thank Anthony Bloom (JPL) for providing the WetCHARTs v1.3.1 emissions product and NIST for
448 funding this project (Project code: 70NANB18H16; Award Number: 70NANB22H219). We thank Kimberly
449 Mueller (NIST) for providing us with model convolutions. Northeast Corridor tower methane observations are
450 available at <https://doi.org/10.18434/M32126> (Karion et al., 2019).

451

452 **Open Research**

453 Methane observations from the Northeast Corridor tower network can be found at
 454 <https://doi.org/10.18434/M32126> (Karion et al., 2019). STILT model data have been described in Lin et al
 455 2003b (<https://doi.org/10.1029/2002JD003161>), and the WRF model data have been described in Skamarock et
 456 al 2008 (<http://dx.doi.org/10.5065/D68S4MVH>). The EDGAR 4.2 data have been obtained from
 457 <http://data.europa.eu/89h/jrc-edgar-emissiontimeseriesv42> and the EDGAR 5.0 have been obtained from
 458 <http://data.europa.eu/89h/488dc3de-f072-4810-ab83-47185158ce2a>. WetCHARTs is described in Bloom et al.,
 459 (2017).

460

461 **References**

- 462 Alvarez, R.A. *et al.* (2012). Greater focus needed on methane leakage from natural gas infrastructure, *Proceedings*
 463 *of the National Academy of Sciences of the United States of America*, 109(17), pp. 6435–6440.
 464 <https://doi.org/10.1073/PNAS.1202407109>
- 465 Alvarez, R.A. *et al.* (2018). Assessment of methane emissions from the U.S. oil and gas supply chain. *Science*,
 466 361(6398), pp. 186–188. <https://doi-org.proxy-um.researchport.umd.edu/10.1126/science.aar7204>
- 467 Bloom, A. *et al.* (2017). A global wetland methane emissions and uncertainty dataset for atmospheric chemical
 468 transport models (WetCHARTs version 1.0). *Geoscientific Model Development*, 10(6), pp. 2141–2156.
 469 <https://doi.org/10.5194/GMD-10-2141-2017>
- 470 Bloomer, B.J., Vinnikov, K.Y. and Dickerson, R.R. (2010). Changes in seasonal and diurnal cycles of ozone and
 471 temperature in the eastern U.S. *Atmospheric Environment*, 44(21–22), pp. 2543–2551.
 472 <https://doi.org/10.1016/J.ATMOSENV.2010.04.031>
- 473 Cambaliza, M.O.L. *et al.* (2015). Quantification and source apportionment of the methane emission flux from the
 474 city of Indianapolis. *Elementa*, 3. <https://doi.org/10.12952/JOURNAL.ELEMENTA.000037>
- 475 Crippa, M. *et al.* (2019). EDGAR v5.0 Greenhouse Gas Emissions. European Commission, Joint Research Centre
 476 (JRC) [Dataset] PID: <http://data.europa.eu/89h/488dc3de-f072-4810-ab83-47185158ce2a>
- 477 Dyer, A.J. (1974). A review of flux-profile relationships,” *Boundary-Layer Meteorology* 1974 7:3, 7(3), pp. 363–
 478 372. <https://doi.org/10.1007/BF00240838>
- 479 *EDGAR - The Emissions Database for Global Atmospheric Research*.
 480 https://edgar.jrc.ec.europa.eu/index.php/dataset_ghg50 (Accessed: May 15, 2022).
- 481 Gallagher, M.E. *et al.* (2015). Natural Gas Pipeline Replacement Programs Reduce Methane Leaks and Improve
 482 Consumer Safety. *Environmental Science & Technology Letters*, 2(10), pp. 286–291.
 483 <https://doi.org/10.1021/acs.estlett.5b00213>
- 484 He, L. *et al.* (2019). Atmospheric Methane Emissions Correlate with Natural Gas Consumption from Residential and
 485 Commercial Sectors in Los Angeles. *Geophysical Research Letters*, 46(14), pp. 8563–8571.
 486 <https://doi.org/10.1029/2019GL083400>
- 487 Hendrick, M.F. *et al.* (2016). Fugitive methane emissions from leak-prone natural gas distribution infrastructure in
 488 urban environments. *Environmental Pollution*, 213, pp. 710–716.
 489 <https://doi.org/10.1016/J.ENVPOL.2016.01.094>
- 490 Horst, T.W. (1999). The footprint for estimation of atmosphere-surface exchange fluxes by profile techniques.
 491 *Boundary-Layer Meteorology*, 90(2), pp. 171–188. <https://doi.org/10.1023/A:1001774726067>
- 492 Huang, Y. *et al.* (2019). Seasonally Resolved Excess Urban Methane Emissions from the Baltimore/Washington,
 493 DC Metropolitan Region. *Environmental Science and Technology*, 53(19), pp. 11285–11293.
 494 <https://doi.org/10.1021/acs.est.9b02782>

- 495 *Inventory of U.S. Greenhouse Gas Emissions and Sinks* | US EPA. [https://www.epa.gov/ghgemissions/inventory-us-](https://www.epa.gov/ghgemissions/inventory-us-greenhouse-gas-emissions-and-sinks)
496 [greenhouse-gas-emissions-and-sinks](https://www.epa.gov/ghgemissions/inventory-us-greenhouse-gas-emissions-and-sinks) (Accessed: March 28, 2022).
- 497 Jackson, R.B. *et al.* (2014). Natural gas pipeline leaks across Washington, DC. *Environmental Science and*
498 *Technology*, 48(3), pp. 2051–2058.
499 https://doi.org/10.1021/ES404474X/ASSET/IMAGES/ES404474X.SOCIAL.JPEG_V03
- 500 Janssens-Maenhout, G. *et al.* (2011). Emissions Database for Global Atmospheric Research, version v4.2 (time-
501 series). European Commission, Joint Research Centre (JRC) [Dataset] PID: [http://data.europa.eu/89h/jrc-](http://data.europa.eu/89h/jrc-edgar-emissiontimeseriesv42)
502 [edgar-emissiontimeseriesv42](http://data.europa.eu/89h/jrc-edgar-emissiontimeseriesv42)
- 503 Janssens-Maenhout, G. *et al.* (2013). Global emission inventories in the Emission Database for Global Atmospheric
504 Research (EDGAR)—Manual (I). *publications.jrc.ec.europa.eu*.
505 <https://doi.org/10.2788/81454>
- 506 *Joint Research Centre Data Catalogue - EDGAR v5.0 Greenhouse Gas Emissions - European Commission*.
507 <https://data.jrc.ec.europa.eu/dataset/488dc3de-f072-4810-ab83-47185158ce2a> (Accessed: May 15, 2022).
- 508 Karion, A. *et al.* (2019). Observations of CO₂, CH₄, and CO mole fractions from the NIST Northeast Corridor
509 urban testbed. <https://doi.org/10.18434/M32126>
- 510 Karion, A. *et al.* (2020). Greenhouse gas observations from the Northeast Corridor tower network. *Earth System*
511 *Science Data*, 12(1), pp. 699–717. <https://doi.org/10.5194/ESSD-12-699-2020>
- 512 Lamb, B.K. *et al.* (2015). Direct measurements show decreasing methane emissions from natural gas local
513 distribution systems in the United States. *Environmental Science and Technology*, 49(8), pp. 5161–5169.
514 <https://doi.org/10.1021/es505116p>
- 515 Lamb, B.K. *et al.* (2016). Direct and Indirect Measurements and Modeling of Methane Emissions in Indianapolis,
516 Indiana. *Environmental Science and Technology*, 50(16), pp. 8910–8917.
517 <https://doi.org/10.1021/acs.est.6b01198>
- 518 Lin, J.C. *et al.* (2003a). A near-field tool for simulating the upstream influence of atmospheric observations: The
519 Stochastic Time-Inverted Lagrangian Transport (STILT) model. *Journal of Geophysical Research:*
520 *Atmospheres*, 108(D16), p. 4493. <https://doi.org/10.1029/2002JD003161>
- 521 Lin, J.C. *et al.* (2003b). A near-field tool for simulating the upstream influence of atmospheric observations: The
522 Stochastic Time-Inverted Lagrangian Transport (STILT) model. *Journal of Geophysical Research:*
523 *Atmospheres*, 108(D16), p. 4493. <https://doi.org/10.1029/2002JD003161>
- 524 Lopez-Coto, I. *et al.* (2017). Tower-based greenhouse gas measurement network design—The National Institute of
525 Standards and Technology Northeast Corridor Testbed. *Advances in Atmospheric Sciences* 2017 34:9,
526 34(9), pp. 1095–1105. <https://doi.org/10.1007/S00376-017-6094-6>
- 527 Lopez-Coto, I. *et al.* (2020). Wintertime CO₂, CH₄, and CO Emissions Estimation for the Washington, DC–
528 Baltimore Metropolitan Area Using an Inverse Modeling Technique. *Environmental Science &*
529 *Technology*, 54(5), 2606–2614. <https://doi.org/10.1021/acs.est.9b06619>
- 530 McKain, K. *et al.* (2015). Methane emissions from natural gas infrastructure and use in the urban region of Boston,
531 Massachusetts. *Proceedings of the National Academy of Sciences of the United States of America*, 112(7),
532 pp. 1941–1946. <https://doi.org/10.1073/PNAS.1416261112>
- 533 Monteiro, V. *et al.* (2022). The impact of the COVID-19 lockdown on greenhouse gases: a multi-city analysis of in
534 situ atmospheric observations. *Environmental Research Communications*, 4(4), p. 041004.
535 <https://doi.org/10.1088/2515-7620/AC66CB>
- 536 Mueller, K. *et al.* (2018). Siting Background Towers to Characterize Incoming Air for Urban Greenhouse Gas
537 Estimation: A Case Study in the Washington, DC/Baltimore Area. *Journal of Geophysical Research:*
538 *Atmospheres*, 123(5), pp. 2910–2926. <https://doi.org/10.1002/2017JD027364>
- 539 Nehrkom, T. *et al.* (2010). Coupled weather research and forecasting—stochastic time-inverted Lagrangian transport
540 (WRF–STILT) model. *Meteorology and Atmospheric Physics* 2010 107:1, 107(1), pp. 51–64.
541 <https://doi.org/10.1007/S00703-010-0068-X>
- 542 Pak, N. *et al.* (2021). The Facility Level and Area Methane Emissions inventory for the Greater Toronto Area
543 (FLAME-GTA). *Atmospheric Environment*, 252, p. 118319.
544 <https://doi.org/10.1016/J.ATMOSENV.2021.118319>
- 545 Patton, E.G., Sullivan, P.P. and Davis, K.J. (2003). The influence of a forest canopy on top-down and bottom-up
546 diffusion in the planetary boundary layer. *Quarterly Journal of the Royal Meteorological Society*,
547 129(590), pp. 1415–1434. <https://doi.org/10.1256/QJ.01.175>
- 548 Peischl, J. *et al.* (2013). Quantifying sources of methane using light alkanes in the Los Angeles basin, California.
549 *Journal of Geophysical Research: Atmospheres*, 118(10), pp. 4974–4990.
550 <https://doi.org/10.1002/JGRD.50413>

- 551 Phillips, N.G. *et al.* (2013). Mapping urban pipeline leaks: Methane leaks across Boston,. *Environmental Pollution*,
552 173, pp. 1–4. <https://doi.org/10.1016/J.ENVPOL.2012.11.003>
- 553 Plant, G. *et al.* (2019). Large Fugitive Methane Emissions from Urban Centers Along the U.S. East Coast.
554 *Geophysical Research Letters*, 46(14), pp. 8500–8507. <https://doi.org/10.1029/2019GL082635>
- 555 Ren, X. *et al.* (2018). Methane Emissions from the Baltimore-Washington Area Based on Airborne Observations:
556 Comparison to Emissions Inventories. *Journal of Geophysical Research: Atmospheres*, 123(16), pp. 8869–
557 8882. <https://doi.org/10.1029/2018JD028851>
- 558 Sargent, M.R. *et al.* (2021). Majority of US urban natural gas emissions unaccounted for in inventories. *Proceedings*
559 *of the National Academy of Sciences of the United States of America*, 118(44).
560 <https://doi.org/10.1073/pnas.2105804118>
- 561 *Sixth Assessment Report — IPCC*. <https://www.ipcc.ch/assessment-report/ar6/> (Accessed: August 19, 2022).
- 562 Skamarock, W.C. *et al.* (2008). A description of the Advanced Research WRF version 3. NCAR Technical note -
563 475+STR. <http://130.203.136.95/viewdoc/summary?doi=10.1.1.484.3656> (Accessed: July 30, 2022).
- 564 Skamarock, W.C. and Klemp, J.B. (2008). A time-split nonhydrostatic atmospheric model for weather research and
565 forecasting applications. *Journal of Computational Physics*, 227(7), pp. 3465–3485.
566 <https://doi.org/10.1016/J.JCP.2007.01.037>
- 567 Turner, A.J. *et al.* (2016). A large increase in U.S. methane emissions over the past decade inferred from satellite
568 data and surface observations. *Geophysical Research Letters*, 43(5), pp. 2218–2224.
569 <https://doi.org/10.1002/2016GL067987>
- 570 *U.S. Census Bureau QuickFacts: United States*.
571 <https://www.census.gov/quickfacts/fact/table/arlingtoncountyvirginia,baltimorecitymaryland/SEX255221>
572 (Accessed: November 29, 2022).
- 573 Verhulst, K.R. *et al.* (2017). Carbon dioxide and methane measurements from the Los Angeles Megacity Carbon
574 Project - Part 1: Calibration, urban enhancements, and uncertainty estimates. *Atmospheric Chemistry and*
575 *Physics*, 17(13), pp. 8313–8341. <https://doi.org/10.5194/ACP-17-8313-2017>
- 576 Weil, J. C., & Horst, T. W. (1992). Footprint estimates for atmospheric flux measurements in the convective
577 boundary layer. *Precipitation Scavenging and Atmosphere-Surface Exchange*, 2, 717-728.
- 578 Weller, Z.D. *et al.* (2022). Environmental Injustices of Leaks from Urban Natural Gas Distribution Systems:
579 Patterns among and within 13 U.S. Metro Areas. *Environmental Science & Technology*, 56(12), 8599-
580 8609. <https://doi.org/10.1021/acs.est.2c00097>
- 581 Weller, Z.D., Hamburg, S.P. and von Fischer, J.C. (2020). A National Estimate of Methane Leakage from Pipeline
582 Mains in Natural Gas Local Distribution Systems. *Environmental Science and Technology*, 54(14), pp.
583 8958–8967. <https://doi.org/10.1021/acs.est.0c00437>
584 https://doi.org/10.1021/ACS.EST.0C00437/ASSET/IMAGES/LARGE/ES0C00437_0006.JPEG.
- 585 Welp, L.R. *et al.* (2013). Design and performance of a Nafion dryer for continuous operation at CO₂ and CH₄ air
586 monitoring sites. *Atmospheric Measurement Techniques*, 6(5), pp. 1217–1226.
587 <https://doi.org/10.5194/AMT-6-1217-2013>
- 588 Wunch, D. *et al.* (2009). Emissions of greenhouse gases from a North American megacity. *Geophysical Research*
589 *Letters*, 36(15). <https://doi.org/10.1029/2009GL039825>
- 590 Wyngaard, J.C. and Brost, R.A., 1984. Top-down and bottom-up diffusion of a scalar in the convective boundary
591 layer. *Journal of Atmospheric Sciences*, 41(1), pp.102-112.
592 [https://doi.org/10.1175/1520-0469\(1984\)041%3C0102:TDABUD%3E2.0.CO;2](https://doi.org/10.1175/1520-0469(1984)041%3C0102:TDABUD%3E2.0.CO;2)
- 593 Yadav, V. *et al.* (2019). Spatio-temporally Resolved Methane Fluxes from the Los Angeles Megacity. *Journal of*
594 *Geophysical Research: Atmospheres*, 124(9), pp. 5131–5148. <https://doi.org/10.1029/2018JD030062>
- 595 Yang, L. *et al.* (2018). A new generation of the United States National Land Cover Database: Requirements,
596 research priorities, design, and implementation strategies. *ISPRS Journal of Photogrammetry and Remote*
597 *Sensing*, 146, pp. 108–123. <https://doi.org/10.1016/J.ISPRSJPRS.2018.09.006>
- 598 Zimmerle, D.J. *et al.* (2015). Methane Emissions from the Natural Gas Transmission and Storage System in the
599 United States. *Environmental Science and Technology*, 49(15), pp. 9374–9383.
600 <https://doi.org/10.1021/acs.est.5b01669>

601

Analysis of the trends in ambient methane in the Baltimore-Washington region and comparison to model output

Sayantana Sahu¹, Anna Karion², Israel Lopez-Coto², Xinrong Ren³, Ross J. Salawitch^{1,4,5}, Russell R. Dickerson^{1,4,5}

1. Department of Chemistry and Biochemistry, University of Maryland, College Park, Maryland, USA
2. National Institute of Standards and Technology, Gaithersburg, Maryland, USA
3. Air Resources Laboratory, National Oceanic and Atmospheric Administration, College Park, Maryland, USA
4. Department of Atmospheric and Oceanic Science, University of Maryland, College Park, Maryland, USA
5. Earth System Science Interdisciplinary Center, University of Maryland, College Park, Maryland, USA
- 6.

Contents of this file

Figures S1 to S5
Tables S1 to S8

Introduction

- The supporting information contains figures of the geographic location of the towers, modeling domain used in our study, methane flux of WetCHARTs members, distribution of methane flux within EDGAR 6.0, diurnal cycle in summer at ARL and NEB.
- The supporting information contains tables on geographic location and inlet heights of the three towers in our study. In addition, it contains the tables on the bias comparison between observations and model outputs a. with 2nd, 5th, 10th, 15th percentiles as

background b. for all hours in summer and winter c. after adding emissions from various WetCHARTs options.

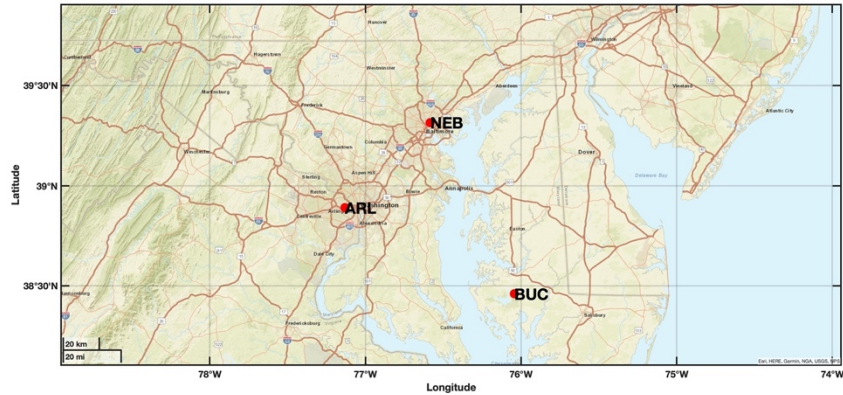


Figure S1: Geographic location of three towers in our study, represented by red dots. Two urban towers NEB (Baltimore, MD), ARL (Arlington, VA) and one rural tower, BUC (Bucktown, MD).

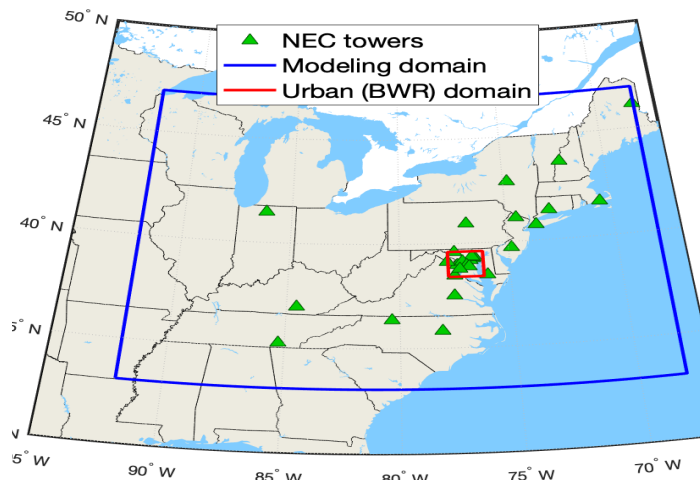


Figure S2: Modeling domains in our study. The larger blue box represents the d01 domain, and the smaller red box represents the BWR.

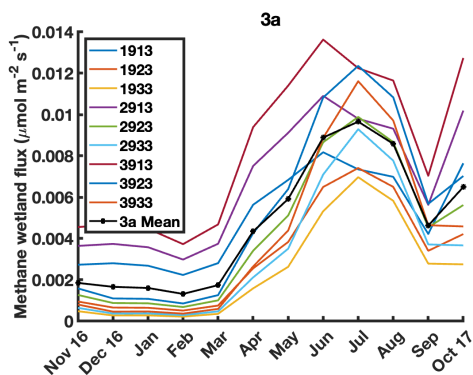


Figure S3a

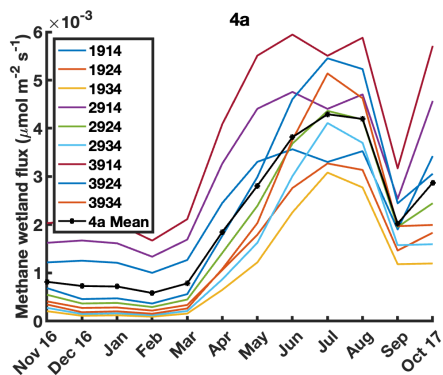


Figure S3b

Figure S3. WetCHARTs members for methane flux for d01 domain. The combination ‘wet3a’ is shown in Figure S3a and ‘wet4a’ in Figure S3b. The black line is the mean of all members in each plot, which is used in our study.

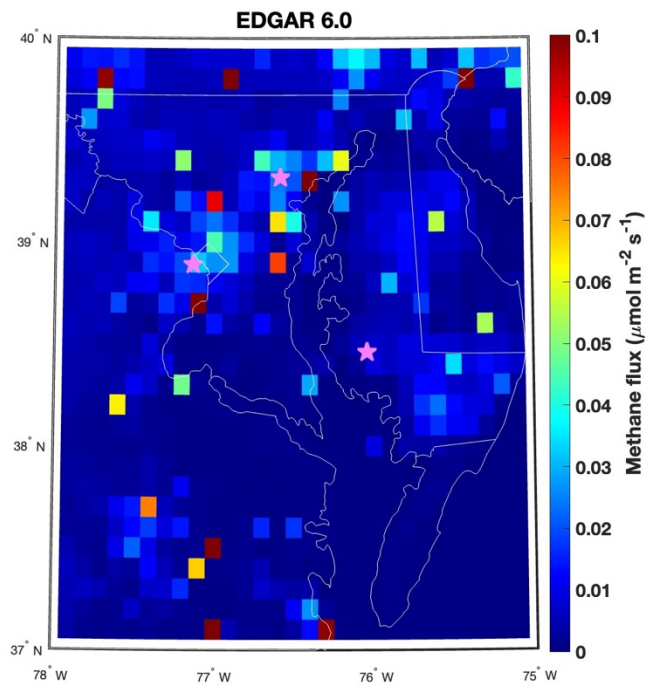


Figure S4

Figure S4: Distribution of CH₄ emission fluxes (in units of $\mu\text{mol}/\text{m}^2/\text{s}$) in EDGAR 6.0 around the towers in the BWR. The pink stars represent the towers in our study. Color axis has been truncated for clarity.

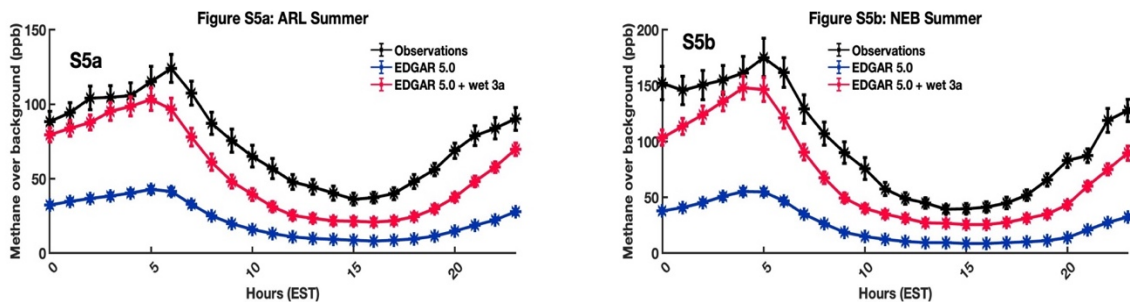


Figure S5. Diurnal cycle of methane at ARL (a) and NEB (b) during summer. The black line represents the hourly averaged methane observed enhancements. The red and blue lines represent the model predicted diurnal cycle using EDGAR 5.0 inventory, with and without wetland emissions respectively.

Tower	Latitude (°)	Longitude (°)	Inlet heights (meters above ground level) (upper/lower)
BUC	38.459699	-76.042970	75/46
NEB	39.315417	-76.583000	67/50
ARL	38.891667	-77.131667	92/50

Table S1: Latitude and longitude of the three towers in our study, along with the inlet heights in the tower.

Tower	Inventory	Season	Percentile	Mean bias (ppb)	NMB
BUC	EDGAR 4.2	winter	5th	-22.26	-0.44
NEB				-42.50	-0.52
ARL				-26.97	-0.40
BUC				-35.59	-0.51

NEB	EDGAR 4.2	winter	2nd	-42.22	-0.49
ARL				-38.07	-0.47
BUC	EDGAR 4.2	winter	10th	-17.89	-0.43
NEB				-35.48	-0.50
ARL				-23.54	-0.40
BUC	EDGAR 4.2	winter	15th	-14.99	-0.40
NEB				-35.34	-0.53
ARL				-22.49	-0.41
BUC	EDGAR 5.0	winter	5th	-37.50	-0.74
NEB				-65.93	-0.80
ARL				-51.78	-0.77
BUC	EDGAR 5.0	winter	2nd	-52.96	-0.76
NEB				-69.39	-0.80
ARL				-65.58	-0.80
BUC	EDGAR 5.0	winter	10th	-30.91	-0.74
NEB				-56.74	-0.80
ARL				-45.30	-0.76
BUC	EDGAR 5.0	winter	15th	-27.61	-0.74
NEB				-55.79	-0.83
ARL				-42.40	-0.78

Table S2: Mean bias and normalized mean bias (NMB) after subtracting the 2nd, 5th, 10th, 15th percentiles from tower methane observations and model results for winter afternoon hours.

Tower	Inventory	Season	Percentile	Mean bias (ppb)	NMB
BUC	EDGAR 4.2	summer	5th	-35.10	-0.60
NEB				-26.98	-0.49
ARL				-18.78	-0.39
BUC	EDGAR 4.2	summer	2nd	-45.99	-0.62
NEB				-28.04	-0.45
ARL				-34.98	-0.52
BUC	EDGAR 4.2	summer	10th	-20.06	-0.50
NEB				-24.33	-0.51
ARL				-17.47	-0.42
BUC	EDGAR 4.2	summer	15th	-15.93	-0.48
NEB				-21.90	-0.52
ARL				-14.59	-0.40
BUC	EDGAR 5.0	summer	5th	-46.38	-0.80
NEB				-43.39	-0.79

ARL				-36.40	-0.75
BUC	EDGAR 5.0	summer	2nd	-59.26	-0.80
NEB				-48.84	-0.78
ARL				-53.92	-0.80
BUC	EDGAR 5.0	summer	10th	-30.79	-0.76
NEB				-38.18	-0.80
ARL				-31.78	-0.76
BUC	EDGAR 5.0	summer	15th	-25.71	-0.77
NEB				-34.02	-0.81
ARL				-28.20	-0.78

Table S3: Same as Table S2 for summer afternoon hours.

Tower	Inventory	Season	Mean bias (ppb)	NMB	r²
BUC	EDGAR 4.2	winter	-22.99	-0.42	0.37
NEB		winter	-49.80	-0.39	0.37
ARL		winter	-21.46	-0.25	0.29
BUC	EDGAR 5.0	winter	-39.12	-0.71	0.37
NEB		winter	-101.10	-0.79	0.34
ARL		winter	-63.57	-0.74	0.30
BUC	EDGAR 4.2	summer	-35.10	-0.60	0.30
NEB		summer	-26.98	-0.49	0.18
ARL		summer	-18.78	-0.39	0.28
BUC	EDGAR 5.0	summer	-46.38	-0.80	0.36
NEB		summer	-43.39	-0.79	0.22
ARL		summer	-36.40	-0.75	0.36

Table S4: Mean bias (ppb), normalized mean bias, and r² between model (WRF-STILT + EDGAR 4.2 and 5.0) and observations for all hours in summer and winter.

Tower	Inventory	Mean bias (ppb)	NMB	r²
BUC	EDGAR 5.0	-37.50	-0.74	0.29
	EDGAR 5.0 + 3a	-34.33	-0.68	0.30
	EDGAR 5.0 + 3b	-33.81	-0.67	0.29
	EDGAR 5.0 + 4a	-36.21	-0.72	0.30
	EDGAR 5.0 + 4b	-36.20	-0.72	0.30
	EDGAR 5.0 + ma	-35.30	-0.70	0.30
	EDGAR 5.0 + mb	-34.99	-0.69	0.30
NEB	EDGAR 5.0	-65.93	-0.80	0.39
	EDGAR 5.0 + 3a	-63.06	-0.77	0.42
	EDGAR 5.0 + 3b	-63.15	-0.77	0.42
	EDGAR 5.0 + 4a	-64.55	-0.79	0.41
	EDGAR 5.0 + 4b	-64.57	-0.79	0.42
	EDGAR 5.0 + ma	-63.80	-0.78	0.42
	EDGAR 5.0 + mb	-63.90	-0.78	0.42
ARL	EDGAR 5.0	-51.78	-0.77	0.36
	EDGAR 5.0 + 3a	-49.05	-0.73	0.37
	EDGAR 5.0 + 3b	-48.99	-0.73	0.37
	EDGAR 5.0 + 4a	-50.25	-0.75	0.38
	EDGAR 5.0 + 4b	-50.40	-0.75	0.38
	EDGAR 5.0 + ma	-49.65	-0.74	0.38
	EDGAR 5.0 + mb	-49.79	-0.74	0.37

Table S5: Model mean bias, NMB, and r² after adding emissions from different WetCHARTs options (3a, 3b, 4a, 4b, ma, mb as described in the text) for winter afternoon hours.

Tower	Inventory	Mean bias (ppb)	NMB	r²
	EDGAR 5.0	-39.12	-0.71	0.37
	EDGAR 5.0 + 3a	-35.08	-0.63	0.37
	EDGAR 5.0 + 3b	-34.09	-0.62	0.36
	EDGAR 5.0 + 4a	-37.60	-0.68	0.37

BUC	EDGAR 5.0 + 4b	-37.52	-0.68	0.37
	EDGAR 5.0 + ma	-36.29	-0.66	0.37
	EDGAR 5.0 + mb	-35.71	-0.64	0.37
NEB	EDGAR 5.0	-101.10	-0.7931	0.35
	EDGAR 5.0 + 3a	-96.84	-0.76	0.36
	EDGAR 5.0 + 3b	-96.92	-0.76	0.36
	EDGAR 5.0 + 4a	-99.06	-0.78	0.36
	EDGAR 5.0 + 4b	-98.95	-0.78	0.36
	EDGAR 5.0 + ma	-97.95	-0.77	0.36
	EDGAR 5.0 + mb	-98.04	-0.77	0.36
ARL	EDGAR 5.0	-63.57	-0.74	0.30
	EDGAR 5.0 + 3a	-59.67	-0.70	0.32
	EDGAR 5.0 + 3b	-59.86	-0.70	0.31
	EDGAR 5.0 + 4a	-61.35	-0.72	0.32
	EDGAR 5.0 + 4b	-61.62	-0.72	0.31
	EDGAR 5.0 + ma	-60.53	-0.71	0.32
	EDGAR 5.0 + mb	-60.73	-0.71	0.31

Table S6: Same as Table S5 for all hours in winter.

Tower	Inventory	Mean bias (ppb)	Normalized mean bias	r²
BUC	EDGAR 5.0	-46.38	-0.80	0.36
	EDGAR 5.0 + 3a	-20.78	-0.36	0.081
	EDGAR 5.0 + 3b	-18.77	-0.32	0.073
	EDGAR 5.0 + 4a	-36.35	-0.63	0.16
	EDGAR 5.0 + 4b	-35.83	-0.62	0.16
	EDGAR 5.0 + ma	-28.86	-0.50	0.11
	EDGAR 5.0 + mb	-27.91	-0.48	0.11
	EDGAR 5.0	-43.39	-0.79	0.22
	EDGAR 5.0 + 3a	-22.82	-0.41	0.17
	EDGAR 5.0 + 3b	-23.72	-0.43	0.18
	EDGAR 5.0 + 4a	-34.75	-0.63	0.20
	EDGAR 5.0 + 4b	-35.09	-0.64	0.20

NEB	EDGAR 5.0 + ma	-29.31	-0.53	0.19
	EDGAR 5.0 + mb	-30.10	-0.55	0.19
ARL	EDGAR 5.0	-36.40	-0.75	0.36
	EDGAR 5.0 + 3a	-19.01	-0.39	0.28
	EDGAR 5.0 + 3b	-19.92	-0.41	0.27
	EDGAR 5.0 + 4a	-27.92	-0.58	0.34
	EDGAR 5.0 + 4b	-28.44	-0.59	0.34
	EDGAR 5.0 + ma	-23.39	-0.48	0.31
	EDGAR 5.0 + mb	-24.20	-0.50	0.30

Table S7: Same as Table S5 for summer afternoon hours.

Tower	Inventory	Mean bias (ppb)	Normalized mean bias	r²
BUC	EDGAR 5.0	-62.90	-0.80	0.26
	EDGAR 5.0 + 3a	-22.83	-0.29	0.17
	EDGAR 5.0 + 3b	-12.13	-0.15	0.17
	EDGAR 5.0 + 4a	-46.73	-0.59	0.21
	EDGAR 5.0 + 4b	-46.06	-0.58	0.20
	EDGAR 5.0 + ma	-35.59	-0.45	0.20
	EDGAR 5.0 + mb	-29.88	-0.38	0.20
NEB	EDGAR 5.0	-72.63	-0.74	0.32
	EDGAR 5.0 + 3a	-28.40	-0.29	0.22
	EDGAR 5.0 + 3b	-37.57	-0.38	0.24
	EDGAR 5.0 + 4a	-56.73	-0.58	0.28
	EDGAR 5.0 + 4b	-58.92	-0.60	0.29
	EDGAR 5.0 + ma	-42.93	-0.44	0.25
	EDGAR 5.0 + mb	-48.38	-0.49	0.27
	EDGAR 5.0	-52.63	-0.70	0.28
	EDGAR 5.0 + 3a	-20.65	-0.28	0.23
	EDGAR 5.0 + 3b	-23.83	-0.32	0.19
	EDGAR 5.0 + 4a	-36.52	-0.49	0.29
	EDGAR 5.0 + 4b	-39.77	-0.53	0.26

ARL	EDGAR 5.0 + ma	-28.94	-0.39	0.26
	EDGAR 5.0 + mb	-32.30	-0.43	0.23

Table S8: Same as Table S5 for all hours in summer.

